UC Berkeley
Research Reports

Title
Robust Lateral Control of Heavy Duty Vehicles

Permalink
https://escholarship.org/uc/item/4wd5r18v

Authors
Tai, Meihua
Wang, Jeng-Yu
White, Ryan
et al.

Publication Date
2001-12-01

Robust Lateral Control of Heavy Duty Vehicles

**Meihua Tai, Jeng-Yu Wang, Ryan White,
Masayoshi Tomizuka**
University of California, Berkeley

The contents of this report reflect the views of the authors who are responsible
for the facts and the accuracy of the data presented herein. The contents do not
necessarily reflect the official views or policies of the State of California. This
report does not constitute a standard, specification, or regulation.

CALIFORNIA PARTNERS FOR ADVANCED TRANSIT AND HIGHWAYS

PROJECT TITLE:

Robust Lateral Control of Heavy Duty Vehicles

By

Meihua Tai

Jeng-Yu Wang

Ryan White

Masayoshi Tomizuka

Department of Mechanical Engineering

University of California at Berkeley

Berkeley, CA 94720

Executive Summary

This report summarizes the research results of MOU385, "Robust Lateral Control of Heavy Duty Vehicles". This project represents a continuing effort of PATH's research on automated highway systems (AHS). Research on the lateral control of heavy vehicles for AHS was initiated at PATH in 1993 with MOU129, "Steering and Braking Control of Heavy Duty Vehicles". It was followed by MOU242, "Lateral Control of Commercial Heavy Duty Vehicle", MOU289 (MOU313), "Lateral Control of Heavy Duty Vehicles for Automated Highway Systems (AHS)", and the current project, MOU385. The earlier projects (MOU129 and MOU242) emphasized theoretical aspects, such as model development, analysis of dynamic model from the lateral control point of view, and the robust lateral controller designs. MOU289 (MOU313) focused on the implementational aspects of the lateral controllers: a tractor-semitrailer vehicle was obtained and instrumented with all the necessary hardware and software, open-loop experiments were conducted, system parameters were estimated based on the open-loop tests, and preliminary closed-loop experiments were performed. The current project, MOU385, focuses on designing enhanced robust controllers, experimental validations of the newly designed controllers, and the study of autonomous vehicle following control. To achieve these goals, we have obtained *four* main results.

First, a design methodology with both steering and differential braking as the control inputs is proposed with explicit consideration of model uncertainties and availability of on-board sensors. The differential braking to the rear wheels of the trailer can effectively control the yaw motion of the trailer. Simulations show that smaller lateral error at the rear end of the trailer can be achieved under both nominal and perturbed conditions.

Second, it is observed that the road disturbance to a vehicle lateral control system is the coulomb friction to a mechanical system. Based on this observation, two feedforward compensators are proposed which can be used in combination with linear robust controllers to further improve tracking performance of the linear feedback con-

trol systems. It is shown by simulation that the feedforward compensators effectively improve the performances of the linear feedback control systems.

Third, we identified that the sliding mode controller inherently contains a feedforward compensation term and linear feedback terms in addition to the nonlinear terms. The previously designed sliding mode controller, a linear robust controller with feedforward compensation, and the same linear robust controller are implemented on a tractor-semitrailer combination and compared by analysis and by experiments. The experimental results show that the addition of the feedforward compensator to the linear feedback control system lifts the performance upper limit of the linear feedback control system and improves the system performance without adding too much additional complexity in the implementation and tuning of the control parameters. On the other hand, while the sliding mode controller seemingly lifts the performance upper limit of the linear feedback control system with feedforward compensation, its implementation induces other issues such as careful system identification and observer design, and the tuning of the control parameters is not a trivial task.

The fourth result focuses on the autonomous following of heavy duty vehicles. Autonomous following of heavy vehicles has the potential to greatly reduce the costs of operating platoons of trucks. Computer controlled following allows a vehicle to follow at close range, increasing the gas mileage of trucks within the platoon and alleviating some problems related to driver fatigue. The problem of tracking a vehicle's trajectory using a visual scheme with no communication between vehicles is investigated. Maximizing the ability of a single vehicle to track the trajectory of the preceding vehicle will minimize the propagation of errors throughout the platoon. Different techniques for autonomous following lateral control are presented.

Abstract

In this report, achievements under MOU385, robust lateral control of heavy vehicles for automated highway systems are presented. The purposes of this project are: to design new controllers or redesign existing controllers for lateral control of heavy vehicles to improve performance; to evaluate designed controllers by experiments and to study autonomous vehicle following control. Towards this goal, we have obtained three main results during year 2000-2001, which are presented in this report.

Firstly, a coordinated steering and differential braking controller is presented. Both model uncertainties and availability of sensors are explicitly considered in the controller design. Simulations show a better-damped yaw motion of the trailer, which is beneficial for HVs with large lateral motions.

Secondly, an analogy between a vehicle lateral control system and a mechanical system with the coulomb friction observed. Motivated by this observation, two feedforward compensators are proposed which can be used in combination with linear robust controllers to further improve tracking performance of the linear feedback control systems.

Thirdly, extensive experiments has been conducted for the previously designed sliding mode controller and the experimental results are compared with that of a linear controllers and a linear controller with feedforward compensation. It is concluded that the linear robust feedback controller with feedforward compensation is a middle ground between nonlinear robust controller and linear robust feedback controllers with feedforward compensation.

Lastly, solutions to the heavy vehicle autonomous following lateral control problem using a laser scanning radar unit are presented. When mounted on the front of the following tractor, the sensor gives the relative displacement and yaw of the preceding trailer to the tractor (although the ability to measure small relative yaw is quite limited). Given two vehicles within a platoon, there are two reasonable methods for interpolating a trajectory. One is linear and the other assumes constant curvature.

Using these methods, the performance when tracking the preceding trailer with the following tractor's CG is compared to the case when the following tractor uses a measurement of the preceding tractor position as the reference. The results of simulations show the importance of using the same reference point on the preceding vehicle as the regulation point on the following vehicle. The trajectory of the previous trailer can also be stored discretely aboard the following vehicle, and this stored trajectory can be used as a tracking reference for the following trailer.

1 Introduction

Heavy vehicles (HV's) are very important components in transportation systems, and they are gaining increasing attention in the Automated Highway Systems (AHS) research community. The California PATH (Partners for Advanced Transit and Highways) has been playing a leading role in the research of AHS, and the lateral guidance of heavy vehicles for AHS is one of its recent research focuses [18].

Heavy vehicles exhibit much more complex dynamical characteristics than passenger cars. For example, the tractor-semitrailer combination has two units connected by the fifth wheel, and because of that, the roll and pitch motions of the tractor and semitrailer are coupled. The external forces to the vehicle system come from the interactions between tires and road. The tire forces are very complicated functions of many parameters such as road adhesion coefficient, tire velocity, and tire vertical force. Because of the higher center of gravity of heavy vehicles, the load transfer effect is more significant than in passenger vehicles. Moreover, different cargo and different loading configurations exert different forces on each tire of the heavy vehicle. All of these imply that robust control schemes must be used to assure the stability of the closed-loop automated steering control system in the presence of model uncertainties. Some robust controllers were already designed under previous PATH projects. The purpose of the current project is to design new controllers or redesign existing controllers for actual implementation and experimentation. As it always has been, both linear and nonlinear approaches are studied.

The primary control input for lateral control of automated HVs is the front wheel steering angle. Another possible control input is the differential braking force to the rear wheels of the trailer. Differential braking generates a torque, that can be used to control the yaw motion of the trailer. It can effectively deal with yaw instability modes of the trailer such as fish-tailing. A robust linear steering and differential braking MIMO controller is designed using the H_∞ loop-shaping methodology.

Coordinated steering and braking control of HV's in the AHS was first proposed by

Chen and Tomizuka in [11], where the input-output linearization and back-stepping [23] were applied. In this approach, the modeling uncertainties were not explicitly considered. Furthermore, all vehicle state variables must be accessible to implement the controller in [11], which makes the approach impractical depending on the availability of sensors and presence of measurement noise.

In the proposed approach, only 1) the articulation angle, 2) the lateral errors at the front and rear axle of the tractor, and 3) either the angular velocities of the rear wheels of the trailer or the brake line pressure signals, are assumed to be available for the synthesis of control inputs. In actual implementation, the lateral errors at the virtual look-ahead position is obtained from two magnetometers, which are located at the front and rear ends of the tractor. The articulation angle is obtained from a string gauge mounted on the fifth wheel. The controller is designed to ensure robustness to model uncertainties due to the variations in v (vehicle longitudinal speed), μ (road adhesion coefficient), and m_2 (cargo load in the trailer). Closed-loop simulation results show the robustness of the proposed controller and the resulting smaller lateral error at the trailer end when compared to the controller using the steering input only. More damped transient responses of articulation angle when using the steering and braking control also improve the yaw stability of the trailer.

We observe an analogy between the vehicle lateral control system and a mechanical system with a coulomb friction. Motivated by this observation, we propose to use a feedforward compensator to augment the linear robust feedback controllers for reducing lateral tracking errors while sustaining a reasonable customer comfort. Two feedforward compensators are designed: a fixed-gain feedforward compensator and an adaptive feedforward compensator. Simulation results show that the feedforward compensation effectively reduces the lateral tracking error.

By analyzing the contributing terms of the known nonlinearities which are fed back in most of the nonlinear controllers, we found that the known nonlinear terms actually involve a feedforward compensation term corresponding to fixed-gain feedfor-

2

ward compensation.An extensive comparative experiments are conducted for a sliding mode controller, a linear robust feedback controller with feedforward compensation, and a linear controller. The experimental results show that, the addition of the feedforward compensator to the linear feedback control system lifts the performance upper limit of the linear feedback control system and improves the system performance without adding too much complexity in the implementation and tuning of the control parameters. On the other hand, while the sliding mode controller seemingly lifts the upper limit of the linear feedback control system with feedforward compensation, the implementation induces other issues such as careful system identification and observer design, and the tuning of the control parameters is not a trivial task. It is concluded that a feedforward compensation in addition to a robust linear feedback controller is a mid-point between nonlinear controllers and linear robust controllers in terms of the ease of implementation and the improved control system performance.

Autonomous following of heavy vehicles has the potential to greatly reduce the costs of operating platoons of trucks. It allows one vehicle to follow another at close range, increasing the gas mileage of trucks within the platoon and alleviating some problems related to driver fatigue (eg. [12, 14, 15]). A laser scanning radar unit, mounted on the front of the tractor, is used to determine the relative position and yaw of the preceding trailer, thereby eliminating the need for a road infrastructure in the lateral control of platoons.

The development of simple autonomous following lateral control techniques without inter-vehicle communication is investigated. It is assumed that the longitudinal control of the vehicles within the platoon is already in place. Tracking the preceding trailer's trajectory with the following tractor's CG is initially discussed. The reference trajectory is based on the measured relative position of the preceding trailer, and the performance of linearly interpolating the reference is compared to that of constant curvature interpolation. The relative yaw is used to project the position of the 5th wheel (hitch) of the preceding tractor, giving a reference trajectory that

3

eliminates the offtracking behavior of the trailer. While this type of control may not be fully implementable due to poor measurement resolution of the relative yaw, it shows the importance of tracking the reference trajectory generated by a point on the preceding vehicle with the same point on the following vehicle. The discrete storage of the preceding trailer trajectory is also briefly discussed along with the possibility of using this trajectory as a reference for the following trailer to track.

The remainder of this report is organized as follows. Design of the differential braking controller is presented in Section 2 with closed-loop simulation results. Section 3 presents the design of feedforward compensators and it is tested by simulation in combination with linear robust feedback controller. Comparative experimental result of linear and nonlinear robust controllers are presented in Section 4. Autonomous following control is described in Section 5. Finally, Section 6 gives the conclusions.

2 Robust Coordinated Steering and Differential Braking Control

2.1 Vehicle Control Model with Two Control Inputs

To introduce the differential braking force on the rear wheels of the trailer as another control input, the linearized control model in [3] is reformulated as:

$$
\begin{aligned}
\frac{d}{dt}x_p &= \begin{bmatrix} 0 & I \\ -M^{-1}K & -M^{-1}D \end{bmatrix} x_p + \begin{bmatrix} 0 \\ M^{-1}H \end{bmatrix} \begin{bmatrix} \delta \\ T \end{bmatrix} \\
&\quad + \begin{bmatrix} 0 \\ M^{-1}E_1 \end{bmatrix} \dot{\epsilon}_d + \begin{bmatrix} 0 \\ M^{-1}E_2 \end{bmatrix} \ddot{\epsilon}_d \\
&= A_r x_p + B_r u + G_1 \dot{\epsilon}_d + G_2 \ddot{\epsilon}_d,
\end{aligned}
\tag{1}
$$

4

where M, K, D, E_1, E_2, and x_p are shown in Appendix and

$$H = \begin{bmatrix} 2C_{\alpha_f} & 0 \\ 2l_1 C_{\alpha_f} & \frac{T_{w3}}{2} \\ 0 & \frac{T_{w3}}{2} \end{bmatrix}. \tag{2}$$

δ is the front wheel steering angle and T is the difference between the left and right longitudinal tire forces at the rear wheels of the trailer.

2.1.1 Selection of controlled outputs

Only two outputs can be independently controlled by two control inputs. The analyses presented in [1] suggest that the output of a virtual lateral error sensor located at d_s meters ahead of the tractor's center of gravity: i.e.,

$$y_s = y_r + d_s \epsilon_r \tag{3}$$

is a good candidate as the first controlled output. The virtual sensor scheme presents a transparent tradeoff between lateral error at the tractor's CG and yaw rate damping. When d_s is large, the virtual sensor is located ahead of the front bumper of the tractor, and y_s must be synthesized from the outputs of the magnetometers at the front and rear ends of the tractor. To have a larger phase lead around the cross-over frequency of the dynamic response from δ to y_s, $d_s = 8$ m is chosen. y_s essentially inherits the dynamics of the tractor only. The information about the yaw motion of the trailer can be obtained from the measurement of the articulation angle (ϵ_f) or the lateral error at the trailer rear end (y_{s3}). In other words, there are two possible choices for the second controlled output, or equivalently, two sets of controlled output candidates as shown in Table 1. To decide which set is preferable to the controller design, the inputs and candidate measurements are scaled to make the comparison meaningful and simplify the selection of weighting functions for loop-shaping.

• **Scaling**

y_s and ϵ_f are scaled by $y_{smax} = 0.2$ m (similarly for y_{s3}) and $\epsilon_{fmax} = 5$ deg. The

Table 1: Minimum singular values for the two candidate output sets

Set No.	Candidate controlled outputs	$\underline{\sigma}(G_{steady-state})$
1	y_s and ϵ_f	0.469
2	y_s and y_{s3}	0.164

inputs are scaled by their expected ranges of operation; $10\ deg$ for δ and $10^5\ N$ for T (approximately 0.26 of tire slip ratio). Denoting the unscaled dynamics by $\hat{G}(s)$, the scaled nominal plant, $G(s)$, is given by

$$G(s) = D_e^{-1}\hat{G}(s)D_u, \tag{4}$$

where $D_e = \begin{bmatrix} 0.2 & 0 \\ 0 & \frac{\pi}{36} \end{bmatrix}$ (for Set 1) or $\begin{bmatrix} 0.2 & 0 \\ 0 & 0.2 \end{bmatrix}$ (for Set 2) and $D_u = \begin{bmatrix} \frac{\pi}{18} & 0 \\ 0 & 10^5 \end{bmatrix}$.

● **Steady-state model**

Since the dynamics from δ to y_s includes double-integrator dynamics, its steady-state $(G_{steady-state})$ is analyzed by setting $s = 10^{-6}$ instead of letting $s = 0$ in the transfer functions. With the above scaling, the steady-state model, $y_{all} = G_{all}u$ (where y_{all} contains all the candidate outputs, i.e. $y_{all} = [\ y_s\ \ \epsilon_f\ \ y_{s3}\ ]^T$) and the corresponding RGA (Relative Gain Array)-matrix [27], $\Lambda = G_{all} \times G_{all}^{\dagger\ T}$, are given by

$$G_{all} = \begin{bmatrix} -9.45e12 & 8.61e11 \\ -1.532 & 0.611 \\ -9.45e12 & 8.61e11 \end{bmatrix} \tag{5}$$

$$\Lambda(G_{all}) = \begin{bmatrix} -3.97e11 & 3.97e11 \\ -0.263 & 1.153 \\ 3.97e11 & -3.97e11 \end{bmatrix} \tag{6}$$

6

where $\times$ denotes the element-by-element multiplication, and $\dagger$ is the pseudo-inverse. The singular value decomposition of G_{all} is given by

$$G_{all} = U_0 \Sigma_0 V_0^*, \tag{7}$$

where

$$U_0 = \begin{bmatrix} -0.187 & -0.237 & -0.666 \\ 0 & -0.942 & 0.335 \\ -0.187 & 0.237 & 0.66 \end{bmatrix} \tag{8}$$

$$\Sigma_0 = \begin{bmatrix} 5.06e13 & 0 \\ 0 & 0.498 \\ 0 & 0 \end{bmatrix} \tag{9}$$

$$V_0 = \begin{bmatrix} 0.996 & -0.091 \\ -0.091 & -0.996 \end{bmatrix}. \tag{10}$$

The three row-sums of the RGA-matrix in (6) are

$$\Lambda_\Sigma = \begin{bmatrix} 0.556 & 0.889 & 0.556 \end{bmatrix}. \tag{11}$$

This indicates that outputs 1 and 2 (y_s and ϵ_f) (corresponding to the two largest elements in (11)) should be selected to maximize the projection of the selected outputs onto the space corresponding to the two non-zero singular values. Notice that outputs 2 and 3 (ϵ_f and y_{s3}) also give a large projection. However, both outputs inherit the lateral information of the trailer only, and their combination is not appropriate. Furthermore, the system has a large condition number (see (9)), because there is a double-integrator in the transfer function. This implies that the system is sensitive to unstructured input uncertainties if an inverse-based controller is used.

The selection of outputs should also consider the minimum singular value $\underline{\sigma}(G_{steady-state})$. A large minimum singluar value is preferred, i.e., the choice of outputs y should be
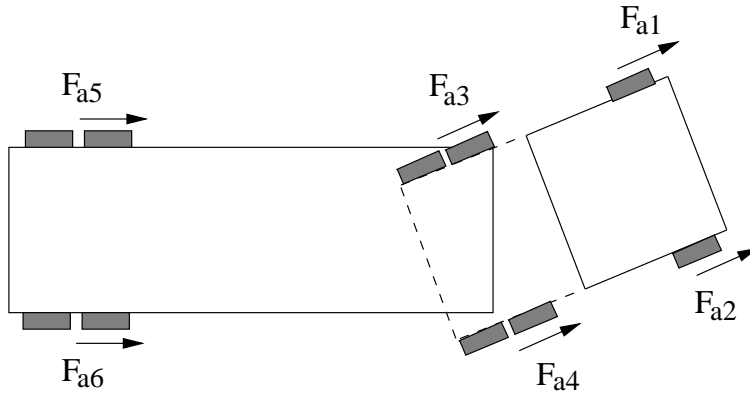
7

Figure 1: Definition of tire longitudinal forces

such that the inputs u have a large effect on y. As shown in Table 1, the minimum singular value of $G_{steady-state}$ is larger for Set 1.

From the above analysis, it was concluded that Set 1 is the best choice for the controlled outputs. That is,

$$y = \left[\begin{array}{cc} y_s & \epsilon_f \end{array} \right]^T. \tag{12}$$

2.2 Strategy for Coordinated Steering and Braking Control

2.2.1 Rear wheel speed sensors on the trailer

Suppose that the rear wheel speed sensors (left and right) are installed on the trailer, which is the case when the trailer is equipped with an Anti-lock Brake System (ABS). Motivated by the work in Chen and Tomizuka [11], the control algorithm is designed in two steps. In the first step, the desired steering command, δ_d, and the desired differential braking force, T_d, are determined by the H_∞ loop-shaping control methodology [3]. T_d is given by $F_{a6d} - F_{a5d}$, where F_{a5d} and F_{a6d} are the desired longitudinal forces at the left and right wheels of the trailer (see Fig. 1)(F_{ai}, for $i = 1 \sim 4$, are the longitudinal forces at the front and rear wheels (left and right) of the tractor and are assumed to be zero). Since F_{a5d} and F_{a6d} are braking forces, they act in a direction opposite to the motion of the wheels (defined as negative). T_d, however, can be positive or negative (counter-clockwise rotation or clockwise rotation around the fifth wheel).

8

If the desired differential braking force is positive, i.e. $T_d > 0$, then $F_{a5d} = -T_d$ and $F_{a6d} = 0$. On the other hand, if $T_d < 0$, $F_{a5d} = 0$ and $F_{a6d} = T_d$. In the second step, the braking torques, τ_5 and τ_6, are determined to generate the desired braking forces, F_{a5d} and F_{a6d}, by utilizing the back-stepping design methodology [23].

The dynamics of the i-th wheel is

$$I_\omega \dot{\omega}_i = -F_{ai} r + \tau_i, \tag{13}$$

where ω_i is the angular velocity of the wheel, r is the radius of tire, F_{ai} is the braking force generated at the tire/ground surface, and τ_i is the braking torque applied at the brake drum of the wheel. The linear tire force can be represented as

$$F_{ai} = C_{lt} \lambda_i, \tag{14}$$

where C_{lt} is the longitudinal stiffness of the trailer's rear wheel, and λ_i is the tire slip ratio defined as

$$\lambda_i = \frac{\omega_i r - v}{v} \tag{15}$$

in the braking case. Combining (13), (14), and (15) gives

$$\dot{F}_{ai} = C_{lt}(-\frac{\omega_i r}{v^2}\dot{v} + \frac{r}{I_\omega v}(-C_{lt}\lambda_i r + \tau_i)). \tag{16}$$

Note that T is determined by the braking force F_{ai}, which can be adjusted only through (16), i.e., the braking torque, τ_i, is the actual control input. τ_i must be adjusted so that the difference between T_d and T is brought to zero, which is the main idea of back-stepping. Two new variables, η_1 and η_2, are defined as

$$\eta_1 = F_{a5} - F_{a5d} \tag{17}$$

and

$$\eta_2 = F_{a6} - F_{a6d}, \tag{18}$$

respectively. Differentiating (17) and (18), and using (16), $\dot{\eta}_1 + k_1\eta_1 = 0$ and $\dot{\eta}_2 + k_2\eta_2 = 0$ are obtained by choosing

$$\tau_5 = C_{lt}\lambda_5 + \frac{I_\omega v}{r}(\frac{\omega_5 r}{v^2}\dot{v} + \frac{1}{C_{lt}}(\dot{F}_{a5d} - k_1\eta_1)) \tag{19}$$

9

and

$$\tau_6 = C_{lt}\lambda_6 + \frac{I_\omega v}{r}(\frac{\omega_6 r}{v^2}\dot{v} + \frac{1}{C_{lt}}(\dot{F}_{a6d} - k_2\eta_2)). \tag{20}$$

Thus, η_1 and η_2 can be brought to zero by choosing positive k_1 and k_2, i.e. T approaches T_d. Notice that there exist uncertain terms in these equations. The nominal values of C_{lt}, angular velocity of the rear wheel of the trailer (ω_5 and ω_6), desired longitudinal forces (F_{a5d} and F_{a6d}), and η_1, η_2 are used to approximate τ_5 and τ_6 in (19) and (20). Approximation errors in determining τ_5 and τ_6 as well as dynamics and uncertainties in the brake subsystem are treated as unmodeled dynamics.

2.2.2 Brake line pressure sensors

If the trailer is not equipped with ABS, speed sensors for the rear wheels of the trailer should be installed. An alternative way to design the braking controller is to use brake line pressure sensors. Notice that the braking torque is actually controlled by the braking pressure (air or hydraulic type) exerted on a moving rod to generate a braking torque against the wheel. Flick [28] conducted an experimental evaluation of braking performance on a similar test vehicle. Based on those results, the braking force and the pressure are related by:

$$F_a \approx 7825.4(P - 0.345) \tag{21}$$

where $F_a[N]$ is the braking force and $P[bar]$ is the control-line pressure. As discussed in the previous subsection, the desired braking forces, F_{a5d} and F_{a6d}, are obtained by the H_∞ controller and therefore, the corresponding desired brake line pressures, P_{5d} and P_{6d}, can be calculated by (21). The dynamics between the command brake pressure and the measured brake pressure can be approximated as a first-order system (0.7 *sec* rising time) with an extra 0.1 *sec* time delay [29].
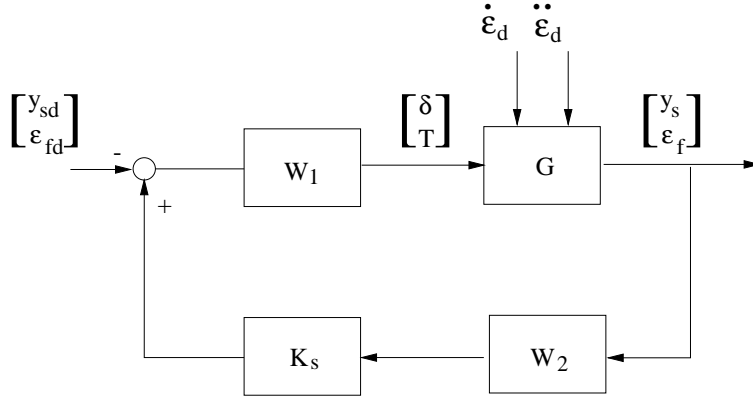
10

Figure 2: Implementation diagram of the steering and braking H_∞ loop-shaping controller

2.3 Robust Coordinated Steering and Differential Braking Controller Design

Figure 2 shows the block-diagram implementation of the proposed H_∞ loop-shaping controller, where W_1 and W_2 are the pre- and post-compensators considered in the H_∞ loop-shaping design, and K_s is the resulting optimal controller. y_{sd} is the desired look-ahead lateral error and is set to zero. ϵ_{fd} is the desired articulation angle and is chosen to be $-\frac{y_{s2}}{l_3}$ to regulate the lateral error at the rear axle of the trailer, where y_{s2} is the lateral error at the rear axle of the tractor (close to the fifth wheel), and l_3 is the distance between the fifth wheel and the rear axle of the trailer.

The singular values of the nominal plant, $G(s)$, are shown in Fig. 3 with dotted lines. They indicate that the low frequency gain should be increased for better steady-state tracking and disturbance rejection. The pre-compensator, W_1, is designed as $W_1 = W_p W_g$ where $W_p = \begin{bmatrix} \frac{2}{0.1s+1} & 0 \\ 0 & \frac{2}{5s+1} \end{bmatrix}$ and $W_g = \begin{bmatrix} 2 & 0 \\ 0 & 2.5 \end{bmatrix}$. Diagonal entries of W_p are low pass filters, which are designed to smooth out the steering action and the differential braking force, thus preventing overheating and fatigue of the steering actuator/column due to high frequency chattering, and also compensating for the slow response of the braking subsystem. W_g is used to adjust the actuator usage.
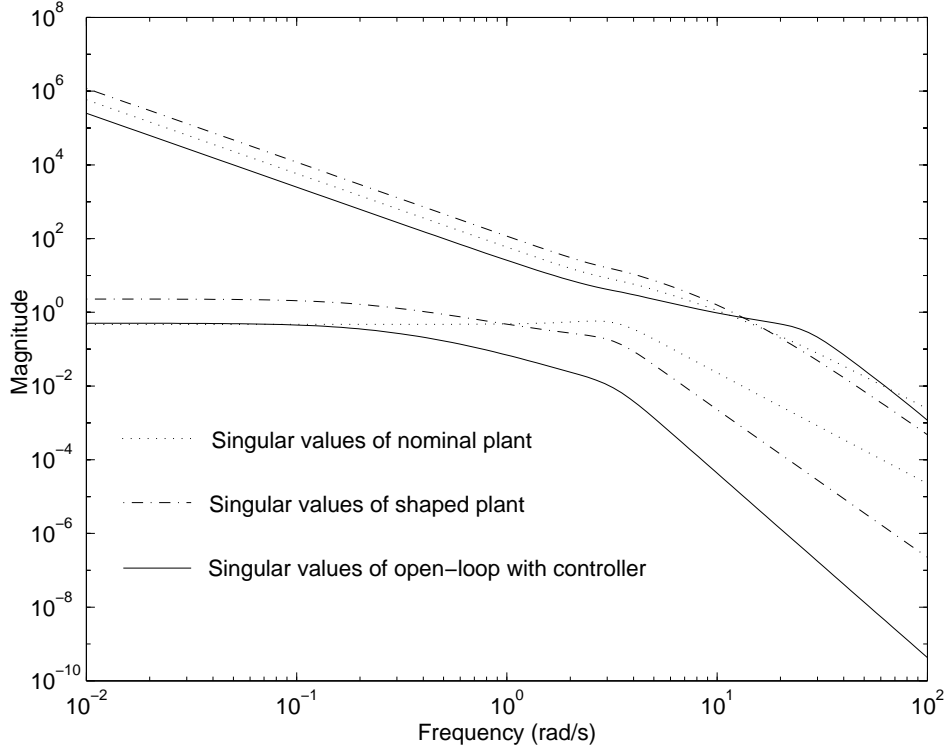
11

Figure 3: Singular values of nominal, shaped plants, and the resulting open-loop dynamics with controller

The post-compensator weight is selected as $W_2 = I_2$. The singular values of the shaped plant, $G_s(s) = W_1 G W_2$, are represented by dash-dotted lines in Fig. 3. The synthesized controller, K_s, is realized together with W_1 and W_2 as shown in Fig. 2. The singular values of the open-loop dynamics with the H_∞ controller are shown in Fig. 3 by solid lines. The slope around the cross-over frequency is -1, which indicates good robustness of the designed controller.

2.4   Closed-Loop Simulations

Closed-loop simulations are performed to compare the two controllers: the proposed steering and braking controller and the steering controller in [3], which was validated by experiments. The road curvature profile used in the simulation is shown in Fig. 4(a). In the controller design, the maneuvering speed is assumed to be constant
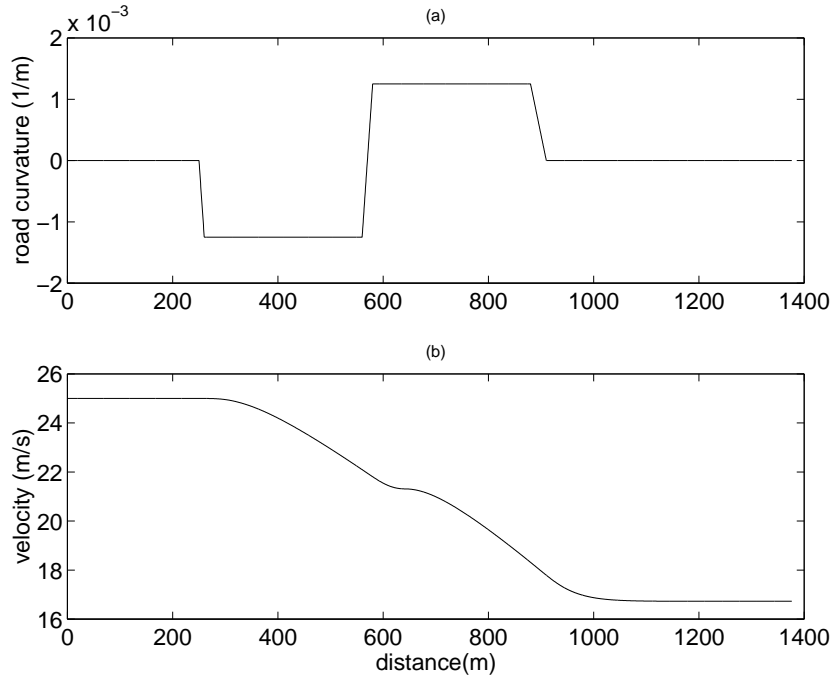
Figure 4: Road curvature (a) and vehicle speed (b)

(25 m/s). The actual speed under the steering and braking control, however, varies as shown in Fig. 4(b). The reduced speed at 260 m results from the effect of applying differential braking. The weighting filters for the steering controller are $W_1(s) = [2]$ and $W_2(s) = \left[\frac{1}{2s+1}\right]$. For the steering and braking controller, $W_1(s)$ and $W_2(s)$ are chosen as mentioned in the previous subsection. The constants, k_1 and k_2, in the design of the steering and braking controller with rear wheel speed sensors are both set to 10. The performance of the steering and braking controller with rear wheel speed sensors or brake line pressure sensors is analyzed via simulations to compare with the performance of the steering controller.

The simulation results for the nominal plant are shown in Figs. 5 and 6. Figure 5 shows the nominal performance using the steering controller (the dashed line) and the steering and braking controller with the rear wheel speed sensors (the solid line). Figure 6 also shows the nominal performance but with the brake line pressure sensors for the steering and braking controller. There is not much difference between using
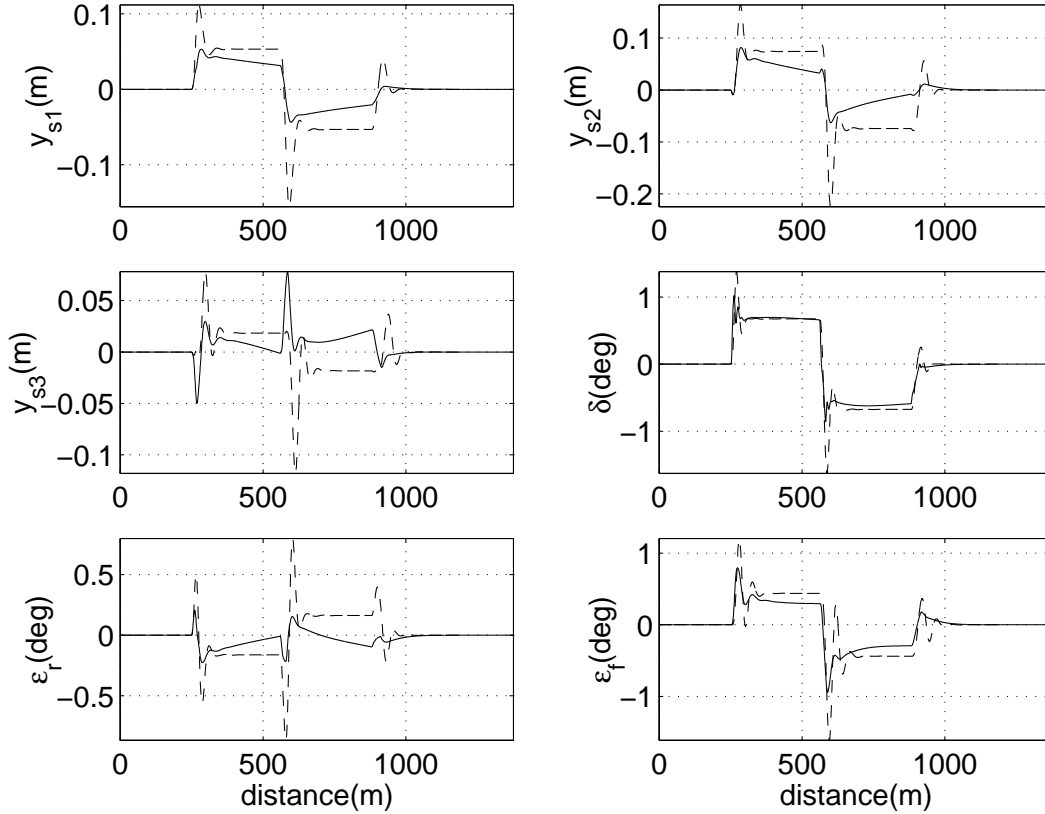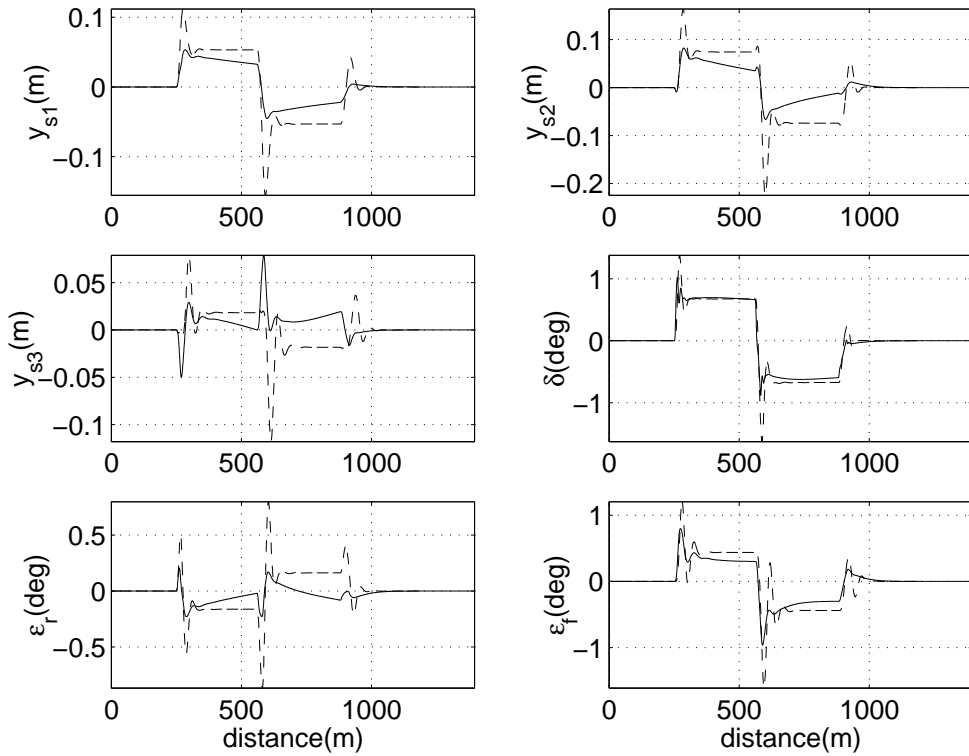
13

Figure 5: Closed-loop simulation under the nominal condition (dashed line: the steering controller)(solid line: the steering and braking controller with rear wheel speed sensors at the trailer)

the rear wheel speed sensors or the brake line pressure sensors in the steering and braking controller. As shown in the figures, the steady-state lateral errors at the three sensor locations are smaller for the steering and braking controllers than the steering controller. Figure 7 shows the brake pressure signals and the braking forces exerted on the rear wheels of the trailer. When the truck enters the first curved section (right turn), F_{a6} (right rear wheel braking force) increases to provide the necessary moment to stabilize the yaw dynamics of the trailer. Similarly, F_{a5} (left rear wheel braking force) increases when truck enters the second curved section (left turn). The resulting tire slip ratio (0.26) is small, thus the braking is operating in the linear region.

The simulation results for a perturbed system ($m_2 = 10455 \cdot 1.5 \ Kg, \mu = 0.7$)

14

Figure 6: Closed-loop simulation under the nominal condition (dashed line: the steering controller)(solid line: the steering and braking controller with brake line pressure sensors)
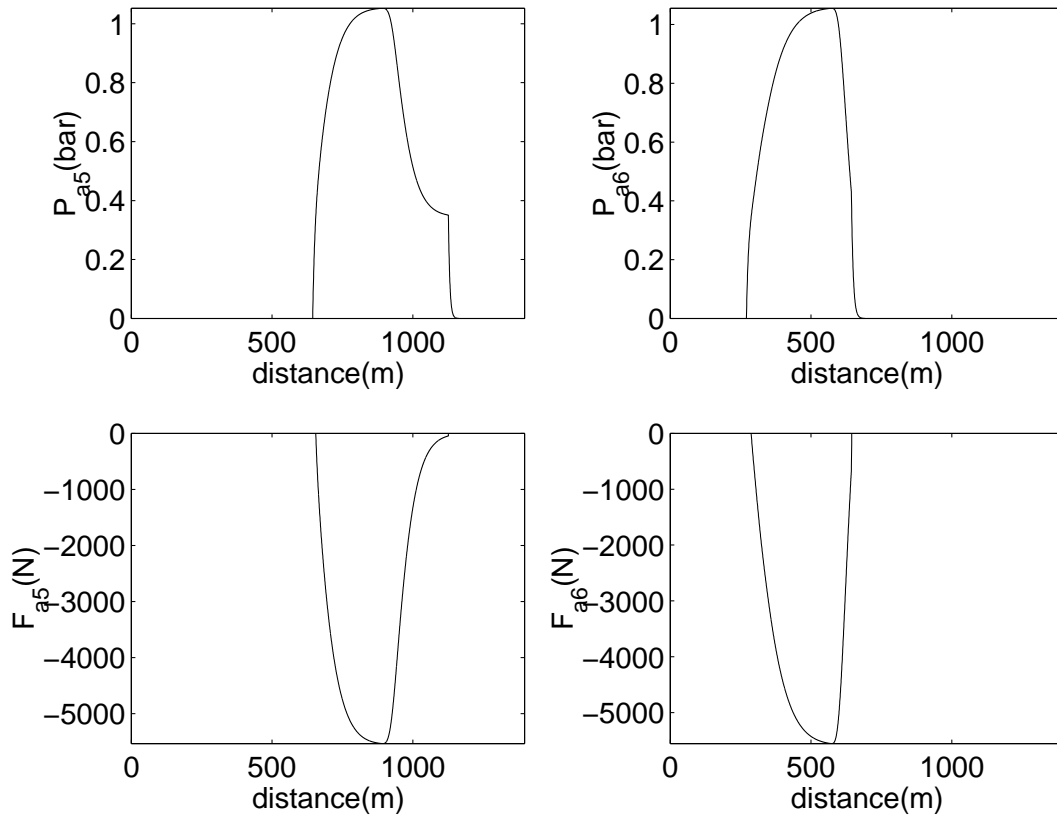
Figure 7: The brake line pressure signals (P_{a5} and P_{a6} for the left and right differential braking actuators, respectively) and the braking forces (F_{a5} and F_{a6} for the left and right braking actuators, respectively)
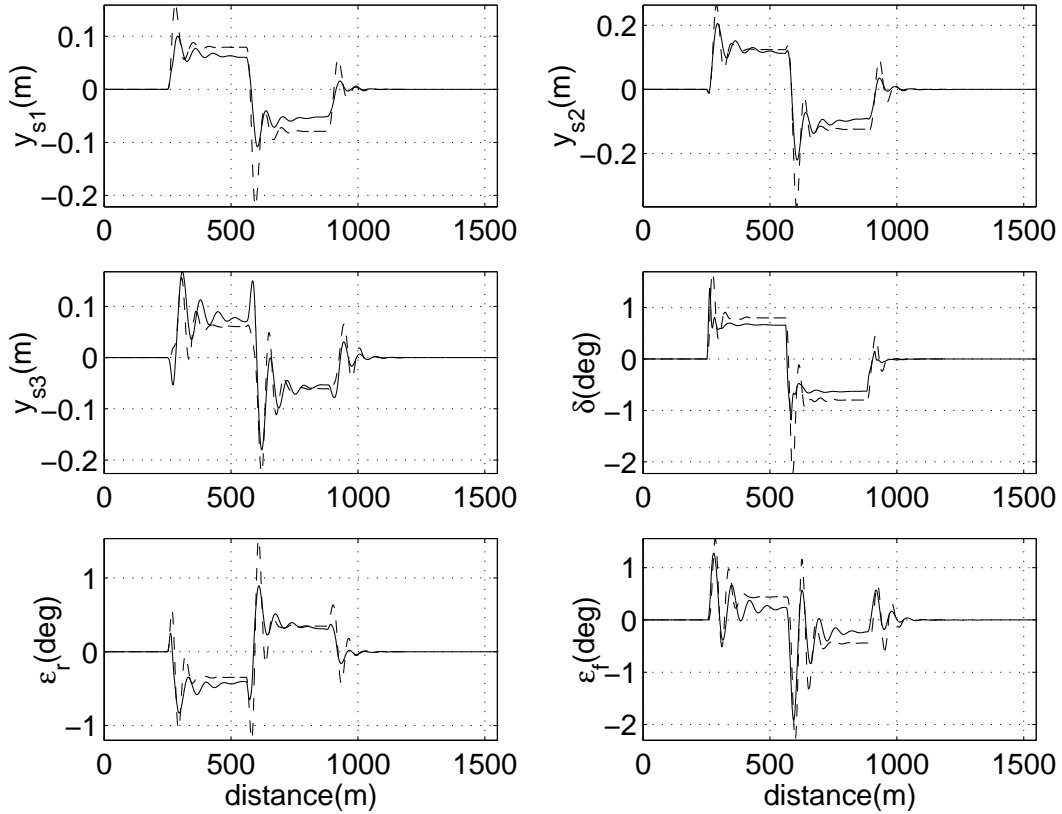
Figure 8: Closed-loop simulation under the perturbed condition ($m_2 = 10455 \cdot 1.5$ kg and $\mu = 0.7$)(Dashed line: the steering controller)(Solid line: the steering and braking controller with brake line pressure sensors)

are shown in Fig. 8 to compare the performance of the steering controller and that of the steering and braking controller using brake line pressure sensors. Parameter uncertainties are also considered in the braking subsystem. For instance, the control gain is reduced by 20 % and the rise time is increased to 1 *sec.* From the simulation results, both controllers are robust to the model uncertainties. With the addition of the differential braking control input, the lateral error at the trailer rear end is further reduced, and the transient response of the articulation angle is more strongly damped, which improves the yaw stability of the trailer.

17

3 Linear Robust Feedback Controller with Feedforward Compensation

Nonlinear controllers are usually designed based on a more detailed nonlinear model of a system and assumes more knowledge of the system to be controlled. Therefore, in theory, they should provide better performances than linear controllers designed based on an approximated, linearized model of the actual system. However, nonlinear controllers are more costly in terms of implementation and sometimes it is impractical to implement them at all. On the other hand, there are rich design methodologies and software tools are available for the design of linear controllers.

In this section, we investigate a possible mid-ground for ease of implementation and high performance by exploring and taking advantages of the inherent structure of the vehicle lateral control system.

3.1 Linear model of a tractor-semitrailer vehicle system

The linear control model of a tractor-semitrailer vehicle system in the road coordinate system is given by

$$M\ddot{q}_r + D\dot{q}_r + Kq_r = F\delta_f + E_1\dot{\varepsilon}_d(t) + E_2\ddot{\varepsilon}_d(t),$$

$$y_s = \left(\begin{array}{ccc} 1 & d_s & 0 \end{array}\right)^T q_r, \tag{22}$$

where

$$q_r = \left(\begin{array}{c} y_s, \varepsilon_r, \varepsilon_f \end{array}\right)^T. \tag{23}$$

The matrices, M, D, K, F, E_1 and E_2, are as given in Appendix A. In the above generalized coordinates, y_r is the lateral displacement of the tractor's center of gravity, ε_r is the tractor's yaw error measured in the road coordinate system and ε_f is the articulation angle. The system input is the tractor's front wheel steering angle δ_f and the system output y_s is the lateral tracking error of the virtual sensor located at the look-ahead distance of d_s. In Eq. (22), $\dot{\varepsilon}_d$ and $\ddot{\varepsilon}_d$ are desired tractor's yaw

rate and rate of change of the desired yaw rate, respectively, and they are treated at disturbances to the system. $\dot{\varepsilon}_d$ is related to the vehicle speed V_x and road curvature ρ by

$$\dot{\varepsilon}_d = V_x\rho. \tag{24}$$

Definie a 6×1 state vector as

$$x_r = \begin{pmatrix} q_r \\ \dot{q}_r \end{pmatrix}. \tag{25}$$

Then the linear state-space model of the vehicle lateral control system is obtained as

$$\begin{aligned} \dot{x}_r &= \begin{pmatrix} 0 & I \\ -M^{-1}K & -M^{-1}D \end{pmatrix} x_r + \begin{pmatrix} 0 \\ M^{-1}F \end{pmatrix} \delta_f \\ &+ \begin{pmatrix} 0 \\ M^{-1}E_1 \end{pmatrix} \dot{\varepsilon}_d + \begin{pmatrix} 0 \\ M^{-1}E_2 \end{pmatrix} \ddot{\varepsilon}_d. \end{aligned} \tag{26}$$

It is noted that the system matrices in Eqs. (22) and (26) depend on the vehicle speed, tire cornering stiffness and load configuration on the trailer. Details of this aspect are documented in [1].

Notice that the desired yaw rate, $\dot{\varepsilon}_d$, appears in the linearized model. In designing linear controllers, the $\dot{\varepsilon}_d$-related terms are treated as disturbances coming from the road, and linear controllers are designed so that they not only reject the road disturbances but also other disturbances such as wind gust. In the presence of such disturbances, the steady-state tracking error is directly affected by the P gain of the controller. The larger the P gain, the smaller the steady-state tracking error. On the other hand, a lager P gain may excite unmodeled dynamics and may induce oscillations.

3.2   Controller design

By examining the sources of the road disturbances and the ways they enter the model equations, we find the following analogy between the lateral dynamics of a vehicle system and the dynamics of a mechanical system with Coulomb friction.
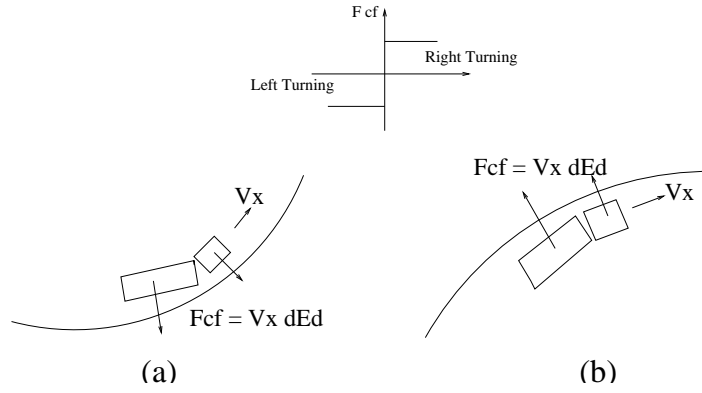
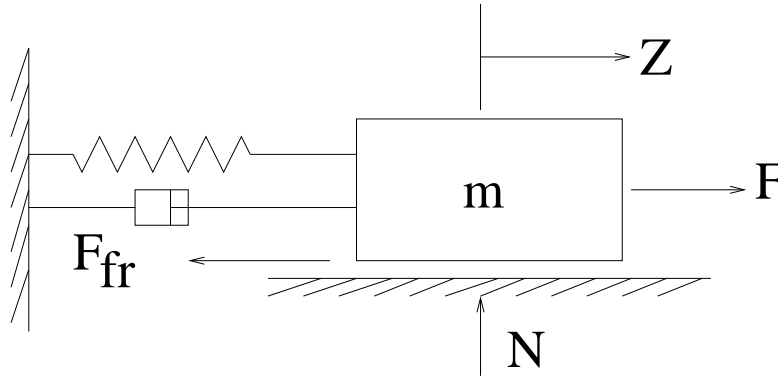Figure 9: Centrifugal Forces of a Vehicle Negotiating a Curve

Figure 10: Coulomb Friction in a Mass-Spring-Damper System

When a vehicle is riding on a straight road, $\dot{\varepsilon}_d$ is zero, and therefore there is no road disturbance. When the vehicle is negotiating a curve and turning left, there are centrifugal forces acting at the centers of gravity of the tractor and of the semitrailer. These centrifugal forces point right and their magnitude is proportional to $V_x\dot{\varepsilon}_d$ as shown in Fig. 9(a). To be precise, the centrifugal forces are proportional to $V_x\dot{\varepsilon}_1$ and $V_x\dot{\varepsilon}_2$, respectively. But, at steady state, we have $\dot{\varepsilon}_1 = \dot{\varepsilon}_2 = \dot{\varepsilon}_d$, and hereafter in this section, we only consider the steady state case. When the vehicle is turning right, the centrifugal forces are proportional to $V_x\dot{\varepsilon}_d$ and they point left as shown in Fig. 9(b). In other words, the centrifugal forces are proportional to $-V_x\dot{\varepsilon}_d$ and are discontinuous.

Recall that, for mechanical systems with Coulomb friction (cf. Fig. 10), the Coulomb friction forces are proportional to $-\dot{x}$ and discontinuous. That is, the centrifugal forces of a vehicle negotiating a curve are analogous to the Coulomb friction forces.

20

For a mechanical system with Coulomb friction, if they can be obtained or esti-
mated, adding a feedforward term to compensate for the disturbances (the friction
forces) is a practical and efficient approach. Motivated by this, we propose to add a
feedforward compensator to a linear feedback control system to attenuate the road
disturbances as shown in Fig. 11. We take the input to the feedforward compensator
as $V_x \dot{\varepsilon}_d$. As such, the feedforward compensator has a built-in switch to turn on and
off the compensator based on needs. That is, when the vehicle is negotiating a curve,
$\dot{\varepsilon}_d$ is nonzero and therefore the feedforward compensator is on, and when the vehicle
is travelling on a straight section, $\dot{\varepsilon}_d$ is zero and therefore the switch is off.

A possible candidate for the feedforward compensator is the inverse dynamics of
the system, from the road disturbances $V_x \dot{\varepsilon}_d$ to the output y_s. But, as we have learned,
the vehicle dynamics has model uncertainties and it may not exactly compensate
for the disturbances as we expect. We propose to use a constant gain feedforward
compensator with the constant equal to the inverse of the P gain of the disturbance
dynamics. This P gain is a function of vehicle inertia and dimensional parameters
as well as tire cornering stiffness. To account for the parametric uncertainties in the
constant feedforward compensator, we introduce an adaptation to the constant gain
based on the lateral tracking error at the c.g. of the tractor.

3.3   Simulation results

We simulated three controllers: a) without feedforward compensation, b) with a con-
stant gain feedforward compensation, and c) with adaptive feedforward compensation.
The feedback controller used in simulations of the three controllers is a linear robust
loop-shaping controller. From Fig. 12, we see that the feedforward compensator effec-
tively reduces the lateral tracking error and provides a smoother control input. The
adaptive feedforward compensator reduces the tracking error even further.
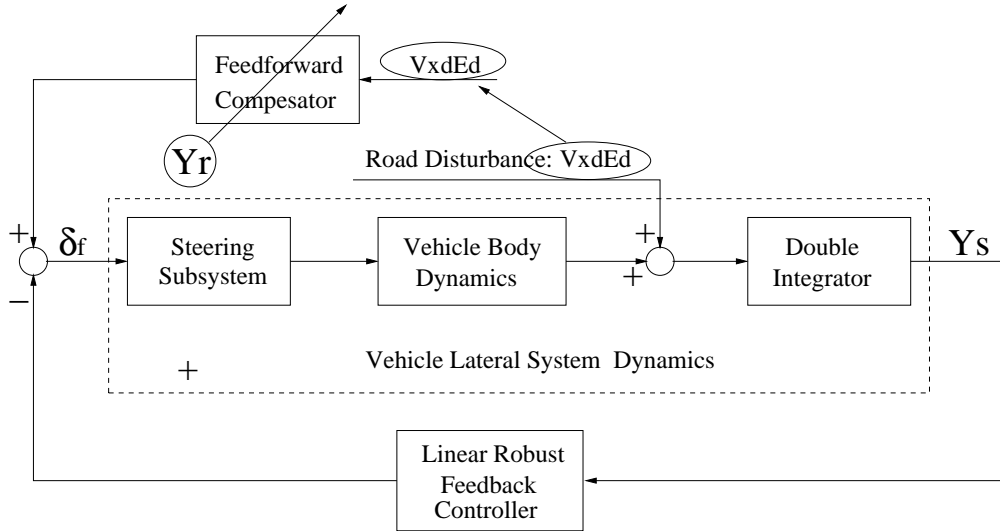
Figure 11: Diagram of Feedforward Compensation for the Lateral Control of a Heavy Vehicle System

3.4 Comparison with nonlinear robust controllers

Recall that the nonlinear robust controllers, such as a sliding mode controller, involve a feedback linearization term. By twice differentiating the output, y_s, the output dynamics of the vehicle lateral control system can be reformatted as

$$
\begin{aligned}
\ddot{y}_s &= \dot{V}_y + d_s\ddot{\varepsilon}_1 + V_x\dot{\varepsilon}_r \\
&= (\dot{V}_y + V_x\dot{\varepsilon}_1 + d_s\ddot{\varepsilon}_1) - V_x\dot{\varepsilon}_d \\
&= f(x) + b(x)\delta_f - V_x\dot{\varepsilon}_d.
\end{aligned}
\tag{27}
$$

Then, the nonlinear controllers have the form of

$$
\begin{aligned}
\delta_f &= -\frac{1}{b(x)}(f(x) - V_x\dot{\varepsilon}_d + \cdots) + \cdots \\
&= \frac{1}{b(x)}(V_x\dot{\varepsilon}_d) - \frac{1}{b(x)}(f(x) + \cdots) + \cdots.
\end{aligned}
\tag{28}
$$

Equation (28) suggests that the nonlinear controllers inherently have a feedforward compensation which corresponds to the fixed gain feedforward control. For comparison, Fig. 13 shows the simulations results of a sliding mode controller and the above mentioned three linear robust controllers. As we can see from the figure, the sliding
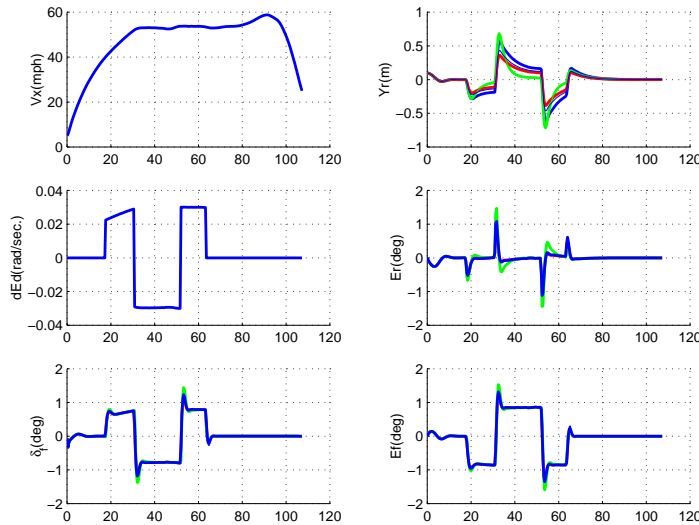
22

Figure 12: Simulation Results of Linear Robust Controllers with Feedforward Compensation: Blue: Without Feedforward Compensation, Red: With Constant Gain Feedforward Compensation, Green: With Adaptive Feedforward Compensation

mode controller offers the best tracking performance as expected. However, as we will see in the following section, the implementation of nonlinear controllers is not trivial and much harder than that of linear controllers. Therefore, linear robust controllers with feedforward compensators are a mid-point between liner feedback controllers and nonlinear controllers from the view point of ease of implementation and control system performance.

4   Comparative Experiments of Lateral Controllers

In this section, we first summarize the previous achievements such as hardware setup and open-loop tests and then present the experimental results of three different controllers, namely, a sliding mode controller, a linear controller with feedforward compensation and a linear controller. These three controllers are compared by analysis and by experiments.
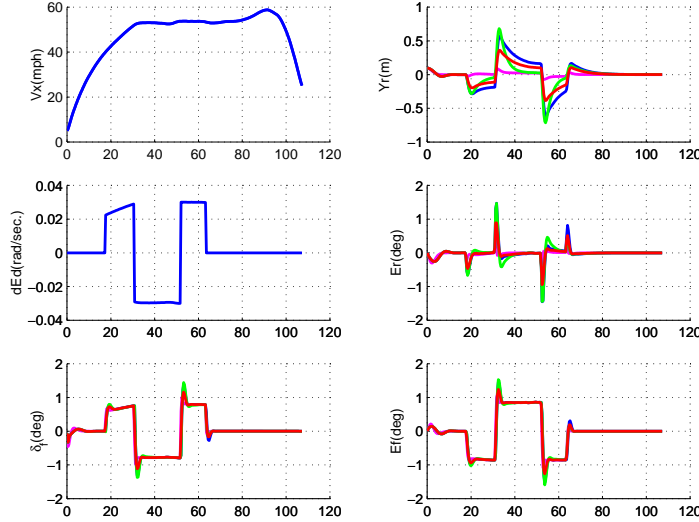
23

Figure 13: Comparison of Nonlinear Controllers with Linear Robust Controllers with Feedforward Compensation: Blue: Without Feedforward Compensation, Red: With Constant Gain Feedforward Compensation, Green: With Adaptive Feedforward Compensation, Magenta: Sliding Mode Controller

4.1 Experimental setup

The experimental vehicle shown in Fig. 14 is a combination of a Freightliner FLD 120 class 8 tractor and a Great Dane semitrailer, completed with a custom designed steering actuator, engine-throttle actuator, brake actuator, and on-board sensors. The sensors and actuators for the lateral and longitudinal control are as shown in Fig. 15.

Steering actuator: The steering actuator is developed by the NSK Corporation of Japan and it is mounted on the steering column as shown in Fig. 16. A robust inner-loop controller is designed for the sub-system represented by the input–output pair, input to the NSK motor driver–steering column angle [25]. A front wheel steering angle sensor is installed on the pitman arm, the output of the hydraulic power assist unit of the steering system.

Brake actuator: The vehicle is installed with brake actuators with electronic control units as shown in Figs. 17 and 18. The electronic unit controls the pressure

Figure 14: Experimental Vehicle

in the brake chambers. A brake chamber diaphragm is connected to an "S" cam by linkages such that an increase of pressure in the brake chamber pushes the brake shoe against the brake drum via the "S" cam and other linkages. At present, only the trailer brake actuators have the left and right independent braking capacity which can be utilized in the lateral controller designs to stabilize the trailer yaw dynamics.

Lateral error sensors: PATH adopted a road-reference system based on magnetic markers. The primary sensors for the lane guidance are the magnetometers. On each of the front end of the tractor, the rear end of the tractor, and the rear end of the semitrailer, there is an array of magnetometers. Each magnetometer array has five magnetometers (see Fig. 19) that allow for a sensing range of $0.8m$ on either side of the road centerline along which magnets are buried in every $1.2m$. An algorithm is designed to obtain the lateral error at the middle sensor location with respect to the road centerline from the signals of the magnetometers in an array.
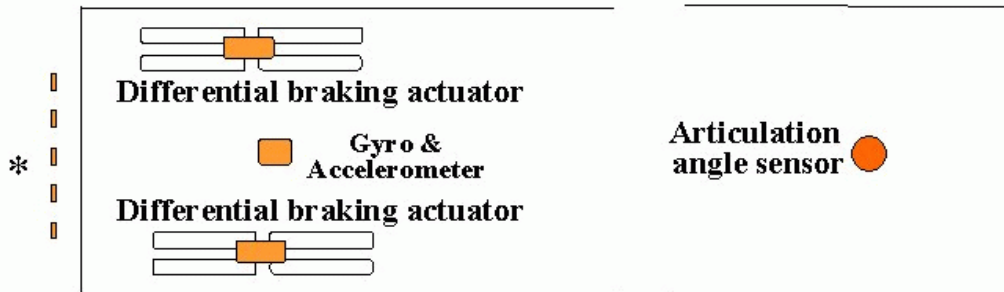
Other sensors: Secondary/subsidiary sensors are also installed either for the controller synthesis or for the fault detection or for the safety and passenger comfort monitoring. They include:
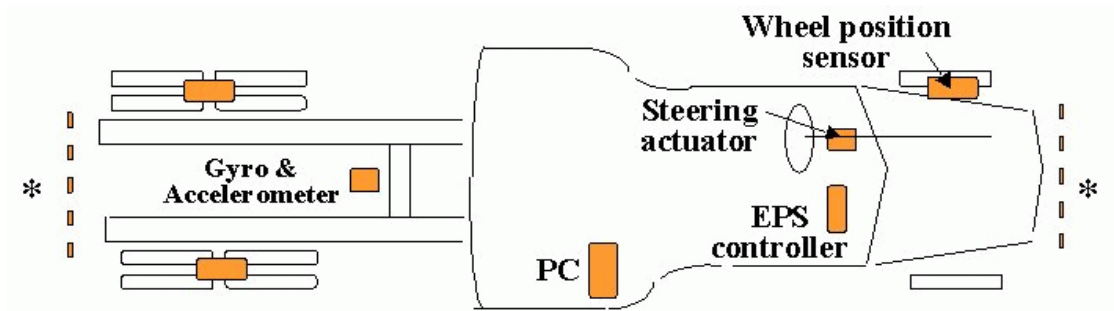
Tractor: Freightlinear FLD 120

*: Magnetormeter array

Semitrailer: Dul axle, 45' aGreat Dane semitrailer

Figure 15: Sensors and Actuators for the Lateral and Longitudinal Control:(1) Front Magnetometer (2)
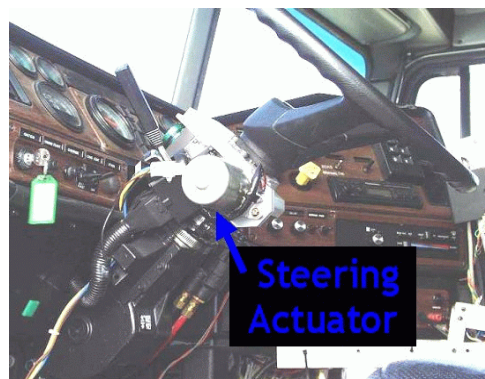

Figure 16: Steering Actuator Mounted on the Steering Column
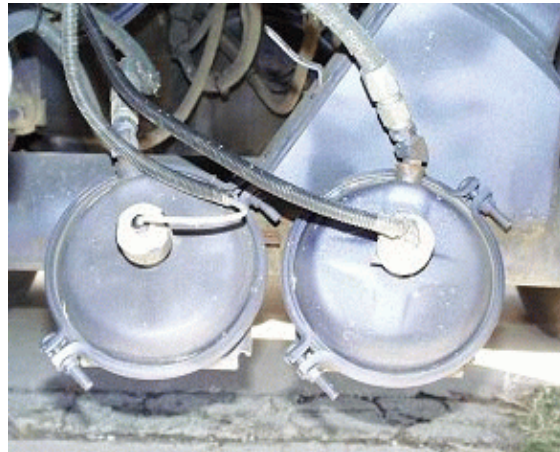
Figure 17: Brake Actuator

Figure 18: Brake Actuator: Air Pressure Transducer

Figure 19: Lateral Position Sensor: Magetometer Array

- accelerometers: one on each of the tractor and semitrailer,

- gyroscopes: one on each of the tractor and semitrailer,

- wheel angle sensor: on the pitman arm, the output shaft of the hydraulic power assist unit of the steering system, and

- articulation angle sensor: around the fifth-wheel.

Hardware interface: A personal computer in the driver cabin of the tractor is in charge of communicating with sensors and actuators through National Instruments' DAQ board. The software for the real time implementation of controllers is based on the previous PATH software architecture and is suitably modified to accommodate new sensors and actuators. The QNX realtime operating system is used.

4.2 Open-loop test and system parameter estimation

Open-loop tests are conducted to estimate some system parameters and verify the linear dynamic model given by Eq. (22). The experiments are conducted at Crows Landing. The test track is about $2000m$ long consisting of 3 curved sections and two straight sections at the beginning and at the end. As we previously pointed out, the linear vehicle model is a Linear Time Varying system (LPV) due to the appearance of the vehicle longitudinal velocity V_x in the system coefficients. To obtain the frequency response of the vehicle lateral dynamics, the frequency sweep tests are conducted at the velocities of $20mph$, $40mph$ and $60mph$. The steering actuator is given a sinusoidal reference command ranging in frequencies from $0.1Hz$ to $2.5Hz$. The recorded output signals are the lateral accelerations and the yaw rates of the tractor and the semitrailer, the articulation angle and the front steering wheel angle.

The system parameters are obtained as follows. Measured dimensional parameters are the distance between tractor's front wheel axle and rear wheel axle ($l_{f1} + l_{r1} =$

$5.35m$), the distance from tractor's rear axle to the fifth-wheel $(l_{r1} - d_{r1} = 3.67)$ and the distance from the fifth-wheel to the semitrailer's rear axle $(d_{f2} + l_{r2} = 10.22m)$. The inertia parameters are provided by the manufacturer: the mass of the tractor $(m_1 = 7956Kg)$ and the mass of the empty semitrailer $(5682Kg)$. The semitrailer is loaded with $5000Kg$ of concretes at the front end, therefore, the total mass of the semitrailer is $m_2 = 10682Kg$. Based on some heavy vehicle design specifications and guidelines, the location of the center of gravity of the tractor and that of the semitrailer are estimated. From the estimation and the dimensional measurements, we have $l_{f1} = 1.68m$, $l_{r1} = 3.67m$, $d_{r1} = 3.56m$, $l_{r2} = 7.32m$ and $d_{f2} = 2.90m$. The rest of the parameters such as the moment of inertia of the tractor (I_{zz}^1) and semitrailer (I_{zz}^2), the tire cornering stiffness $(C_{\alpha f},\ C_{\alpha r}$ and $C_{\alpha t})$ and the location of the accelerometer on the tractor from the estimated c.g. of the tractor (d_s) are estimated by comparing the frequency response of the linear model at the velocities of $20mph$, $40mph$ and $60mph$ with that of the experimental data at the corresponding velocities. The estimated parameters are as follows: $I_{zz}^1 = 32000Kg \cdot m^2$, $I_{zz}^2 = 482790Kg \cdot m^2$, $\mu = 0.75$, $C_{\alpha f} = \mu * 236904N/rad$, $C_{\alpha r} = \mu * 947618N/rad$, $C_{\alpha r} = \mu * 947618N/rad$ and $d_s = -1m$.

As shown in Figs. 20–23, the model, with the above system parameters, matches pretty closely the experimental frequency responses from the steering input to the yaw rate of the tractor, the yaw rate of the semitrailer, the acceleration at the tractor's accelerometer and the articulation angle. These provide us with confidence in designing model based controllers. The experimental data deviates from the linear model at higher frequencies due to the unmodeled dynamics of the road-tire interaction and the suspension system, among others.
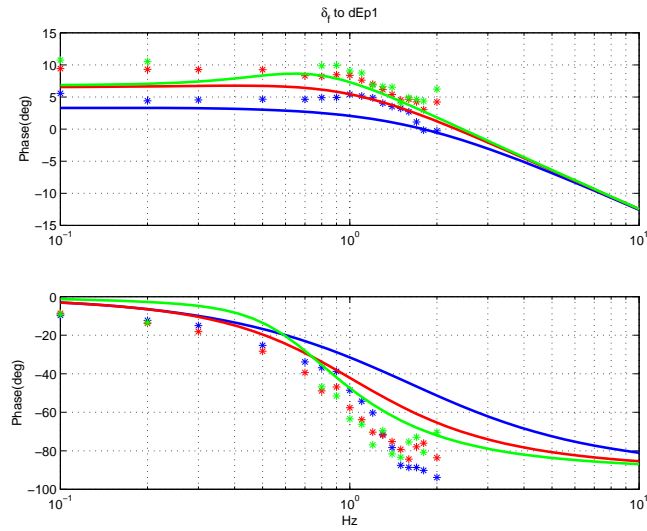
Figure 20: Frequency Response of the Tractor-Semitrailer System from the Steering Wheel to the Yaw Rate of the Tractor: Blue: $20mph$, Red: $40mph$, Green: $60mph$, Solid lines: Model, *: Experiment
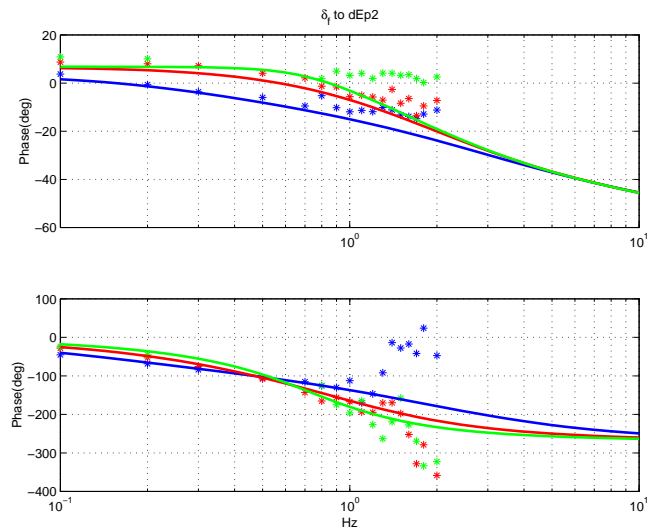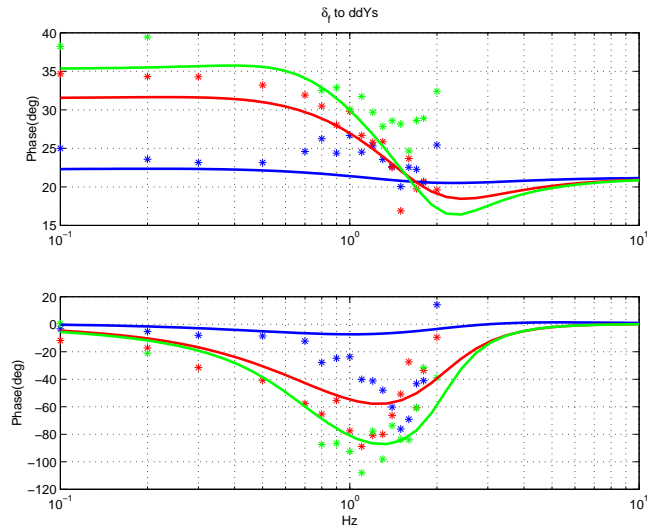

Figure 21: Frequency Response of the Tractor-Semitrailer System from the Steering Wheel to the Yaw Rate of the Semitrailer: Blue: $20mph$, Red: $40mph$, Green: $60mph$, Solid lines: Model, *: Experiment

Figure 22: Frequency Response of the Tractor-Semitrailer System from the Steering Wheel to Acceleration of at the Front Bumper: Blue: $20mph$, Red: $40mph$, Green: $60mph$, Solid lines: Model, *: Experiment
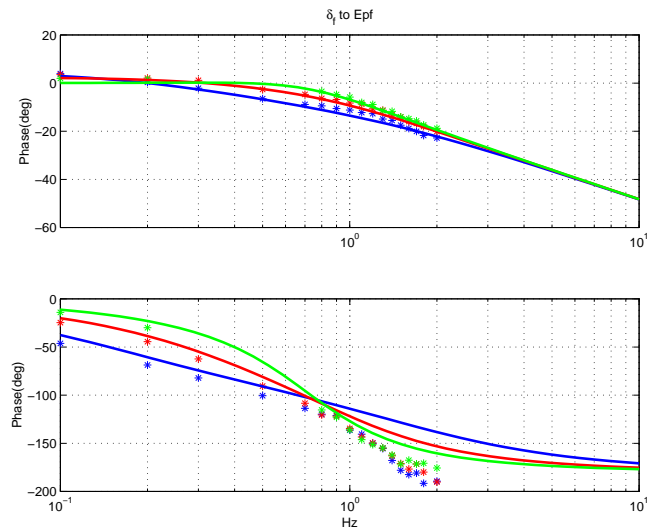

Figure 23: Frequency Response of the Tractor-Semitrailer System from the Steering Wheel to the Articulation Angle: Blue: $20mph$, Red: $40mph$, Green: $60mph$, Solid lines: Model, *: Experiment

4.3 Structural analysis of sliding mode controller

As mentioned in previous section, the output dynamics of the vehicle lateral control system is given by

$$\ddot{y}_s = f(x) + b(x)\delta_f - V_x\dot{\varepsilon}_d + \tilde{f}_2(x), \tag{29}$$

where $\tilde{f}_2(x)$ represents the lumped model uncertainties in the system output, and the nonlinear term $f(x)$ together with $-V_x\dot{\varepsilon}_d$ represents all the modeled dynamics. It is assumed that the model uncertainty, $\tilde{f}_2(x)$, is bounded above by a known smooth function, $\beta(x)$, that is

$$\left\| \tilde{f}_2(x) \right\| \le \beta(x). \tag{30}$$

Then, a sliding mode controller with the sgn function replaced by the sat function is given by [20]

$$\delta_f(x) = -\frac{1}{b(x)} \left(f(x) - V_x\dot{\varepsilon}_d + k_1\mathrm{sat}\left(S/\phi\right) + k_2 S \right) \tag{31}$$

where S is the sliding surface defined by

$$S = \dot{e} + \alpha e, \quad \text{and} \quad e = y_s - y_d, \tag{32}$$

with y_d representing the desired output; k_1 and k_2 are positive control parameters with $k_1 \ge \beta$; and $\phi > 0$ specifies the thickness of the boundary layer.

When the sliding surface is within the boundary layer, i.e., $S \le \phi$, the control input in Eq. (31) is equivalent to

$$\delta_f(x) = -\frac{f(x)}{b(x)} + \frac{1}{b(x)}V_x\dot{\varepsilon}_d - \frac{1}{b(x)}\left(\frac{k_1}{\phi} + k_2\right) S. \tag{33}$$

For the lateral control of heavy vehicles, the desired output is zero, i.e., $y_d = 0$, and the vehicle articulation angle ε_f is very small at highway operations. The $b(x)$ is a function of ε_f only and therefore it is approximated by a constant. Then, Eq. (33) can be approximated by

$$\begin{aligned}
\delta_f(x) &= -\frac{f(x)}{b} + \frac{1}{b}V_x\dot{\varepsilon}_d - \frac{1}{b}\left(\frac{k_1}{\phi} + k_2\right)\dot{y}_s - \frac{\alpha}{b}\left(\frac{k_1}{\phi} + k_2\right)y_s \\
&= -\frac{f(x)}{b} + \frac{1}{b}V_x\dot{\varepsilon}_d - k_3\dot{y}_s - k_3\alpha y_s.
\end{aligned} \tag{34}$$

In Eq. (34), the last two terms represent linear feedback control, the PD control; the second term represents the feedforward compensation whose magnitude is proportional to the centrifugal force; and the first nonlinear terms represents all the modeled dynamics of the vehicle lateral control system including the Coriolis terms as well as terms contributed by the linear tire model. Apparently, the sliding mode controller is doing something more than linear controllers. It consists of three parts: linear feedback control terms, a feedforward compensation term and a nonlinear feedback linearization term. In this section, we compare the following three controllers by experiments.

A. Linear controller,

$$\delta_f = -k_2 \dot{y}_s - k_2 \alpha y_s; \tag{35}$$

B. Linear controller with a fixed gain feedforward compensation,

$$\delta_f = \frac{1}{b} V_x \dot{\varepsilon}_d - k_3 \dot{y}_s - k_3 \alpha y_s; \tag{36}$$

C. Sliding mode controller given by Eq. (34).

The relationships among these three controllers are: controller B is obtained from controller A by adding a fixed gain feedforward compensation and controller C is obtained from controller B by adding a nonlinear term which represents the modeled dynamics of the plant.

4.4   Implementation issues

As we can see from the vehicle model and the sensors installed, not all the system states are measurable. The unmeasured states are synthesized, estimated or observed from the sensor measurements.

Controller A needs two states: y_s and $\dot{y}_s$. The system output y_s at the look-ahead distance d_s is given by

$$y_s = y_r + d_s \varepsilon_r. \tag{37}$$

where y_r and ε_r are obtained from the front and rear magnetometer measurements based on the geometrical relationships. $\dot{y}_s$ is obtained by numerically differentiating y_s.

In addition to the signals that controller A uses, controller B needs two more signals: V_x and $\dot{\varepsilon}_d$. The vehicle longitudinal speed V_x is measured and $\dot{\varepsilon}_d$ is obtained from the equation

$$\dot{\varepsilon}_d = \dot{\varepsilon}_1 - \dot{\varepsilon}_r \tag{38}$$

where the tractor yaw rate $\dot{\varepsilon}_1$ is measured by gyro installed on the tractor and $\dot{\varepsilon}_r$ is obtained by numerically differentiating ε_r. The accuracy of this approach is verified from the experimental data as explained in subsection 4.5.

Nonlinear control algorithms such as controller C depend on the lateral errors measured at the front and rear ends of the tractor as well as many other sensors primarily for the computation of the feedback linearization term. While the lateral error measurements by magnetometers are inherently intermittent, they are least contaminated by the measurement noise, which is one of the reason that the implementation of linear control algorithms has been relatively easy compared to that of nonlinear control algorithms.

While the feedback linearization is a sound analytical idea, the computation of the necessary terms requires many state variables to be measured or estimated. Controller C need 3 additional signals than controller B: V_y, ε_1, ε_f and $\dot{\varepsilon}_f$. The tractor yaw rate $\dot{\varepsilon}_1$ and the articulation angle ε_f are measured. The articulation angle rate, $\dot{\varepsilon}_f$, is obtained from

$$\dot{\varepsilon}_f = \dot{\varepsilon}_2 - \dot{\varepsilon}_1, \tag{39}$$

where the yaw rates of the tractor and the semitrailer, $\dot{\varepsilon}_1$ and $\dot{\varepsilon}_2$, are measured. As for the estimation of the lateral velocity of the tractor's center of gravity, V_y, the lateral error measurements may be fused with the output of the lateral accelerometer, but it is not very satisfactory due to the high noise level in the acceleration signal and bias.

34

However, noticing the following relation,

$$\dot{y}_s = V_y + \varepsilon_r V_x + d_s \dot{\varepsilon}_r, \tag{40}$$

and with the confidence we gained from the estimation of the desired yaw rate, $\dot{\varepsilon}_d$, we can estimated tractor's lateral velocity signal from Eq. (40) as

$$V_y = \dot{y}_s - \varepsilon_r V_x - d_s \dot{\varepsilon}_r, \tag{41}$$

where all the signals on the right hand side of the equation can be obtained as explained in above.

Besides, all the signals but the magnetometer measurements at the front and rear bumper of the tractor are filtered using a lowpass filter.

4.5 Experimental results

The major control objectives in vehicle lateral control are to maintain small lateral errors and to ensure passenger comfort. While there are not many passengers on tractor-semitrailer vehicles, the lateral acceleration and jerk must remain at reasonable levels. In robust nonlinear control algorithms, there is no explicit method of incorporating controller performance in the controller design. The smoothness of the steering input is one of the most important aspects from the viewpoint of public acceptance of automated driving. Most passengers do not like the oscillatory steering action even when it does not adversely affect the lateral acceleration and jerk. Thus, the final tuning of controller parameters must be performed by experiments. Selection of these parameters requires a good understanding of vehicle dynamics, control objectives, and limitations of the actuators.

Experiments are performed on the PATH test track at the Crows landing. The test track consists of three curved sections extended by two straight sections. The radii of the curved sections are $800m$. Figures 24–29 shows the experimental results of controllers A, B and C, respectively. The data are collected on the same day to
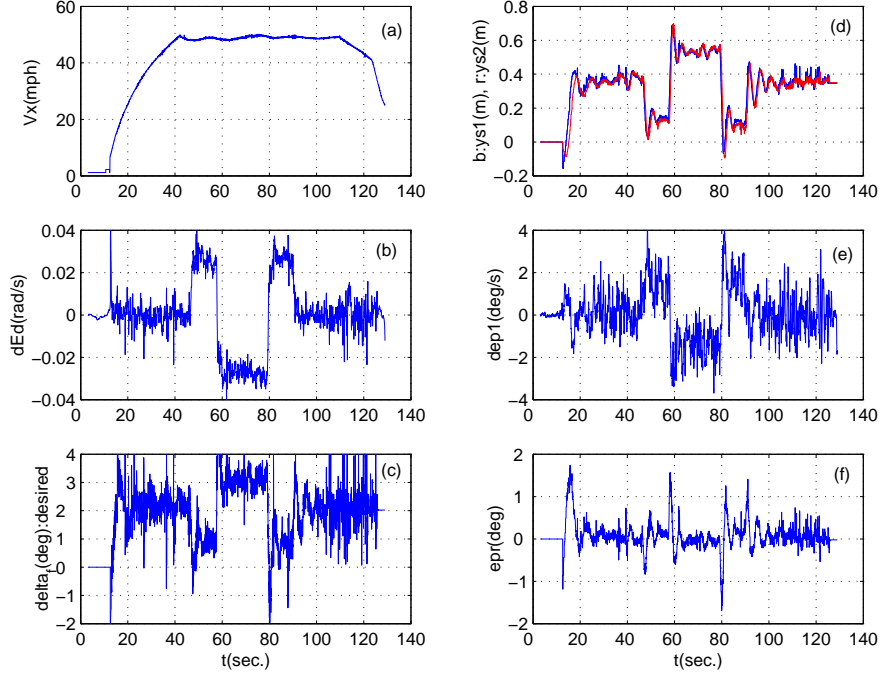
Figure 24: Experimental results of Linear Controller–1

ensure the same experimental environments such as the road condition, the vehicle condition the wind disturbance.

During experiments, the vehicle longitudinal velocity, V_x, is controlled by the driver. In Figs. 24, 26 and 28, the plots (a)–(f) show the vehicle longitudinal speed V_x, the estimated yaw rate $\dot{\varepsilon}_d$, the steering angle command at the handwheel (δ_f) which is the output of the controller, the lateral tracking error at the tractor's front bumper y_{s1} (blue line) and rear bumper y_{s2} (red line), the yaw rate of the tractor $\dot{\varepsilon}_1$ and the orientation of the tractor in the road coordinate system ε_r, respectively.

Notice that in plot (d)-s of Figs. 24, 26 and 28, the lateral tracking error at the front and rear bumpers at the straight sections are nonzero. Also notice that in plot (c)-s of Figs. 24, 26 and 28, at the initial stage when $V_x = 0mph$, there is a large steering action. The latter is because, when we switch to the automatic driving mode, the inner-loop controller calibrates the front steering wheel to the "zero" position, i.e., the straight driving position, before turning on the lateral controller, and for the inner-loop controller to calibrate the steering wheel, the driver is supposed to
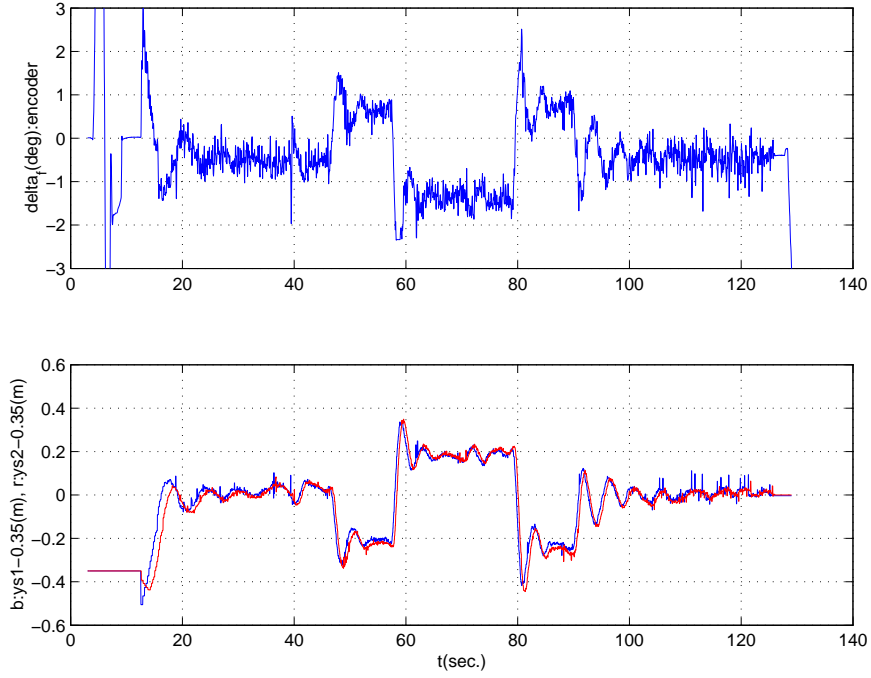
36

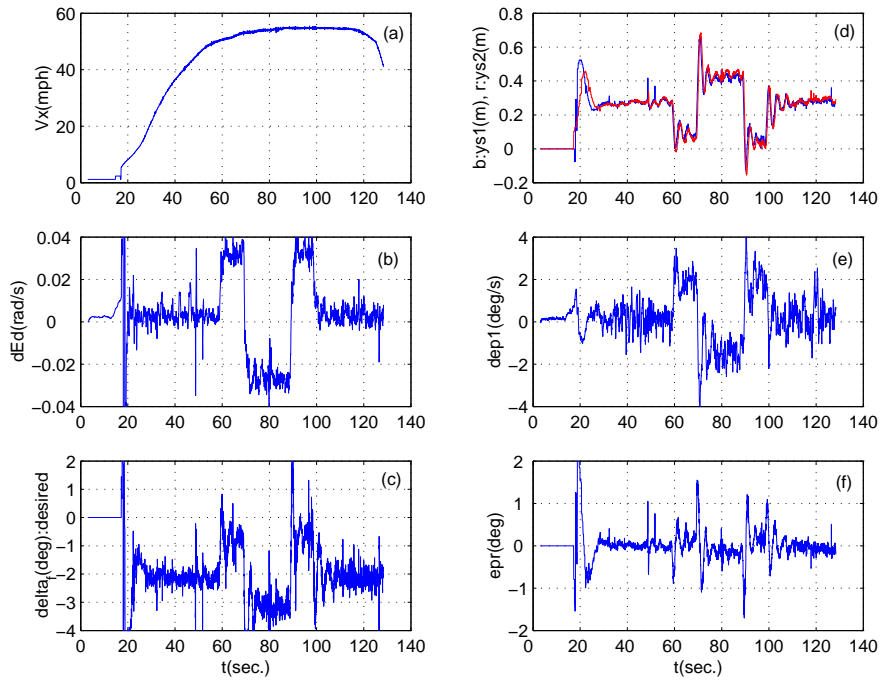Figure 25: Experimental results of Linear Controller–2

Figure 26: Experimental results of Linear Controller with Feedforward Compensation–1
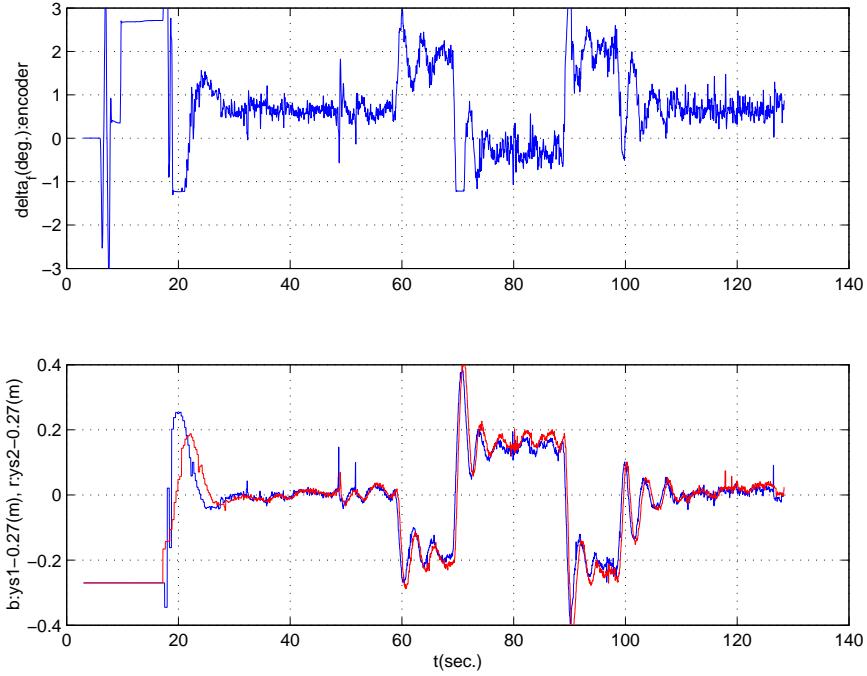
Figure 27: Experimental results of Linear Controller with Feedforward Compensation–2
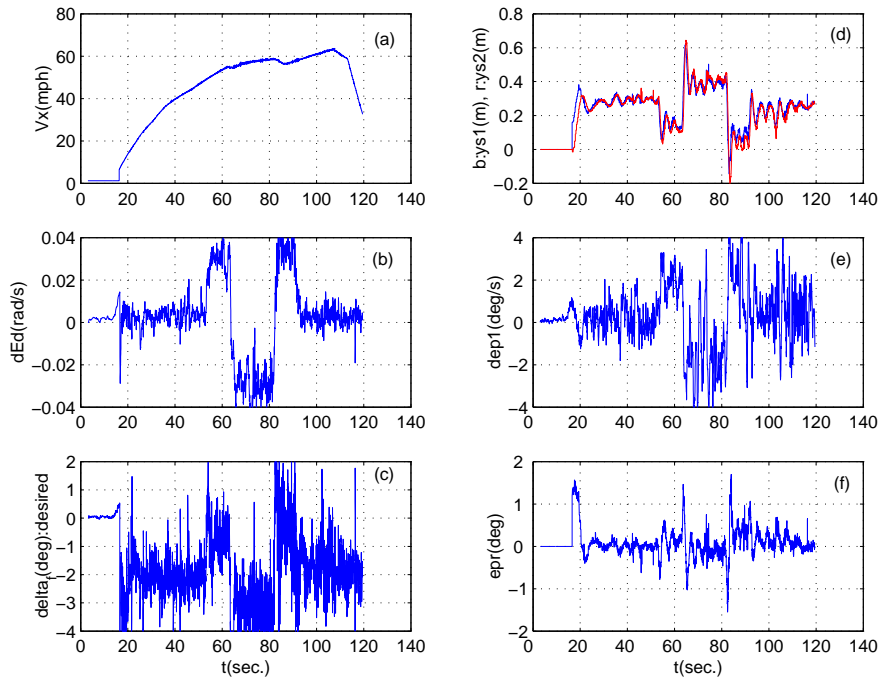

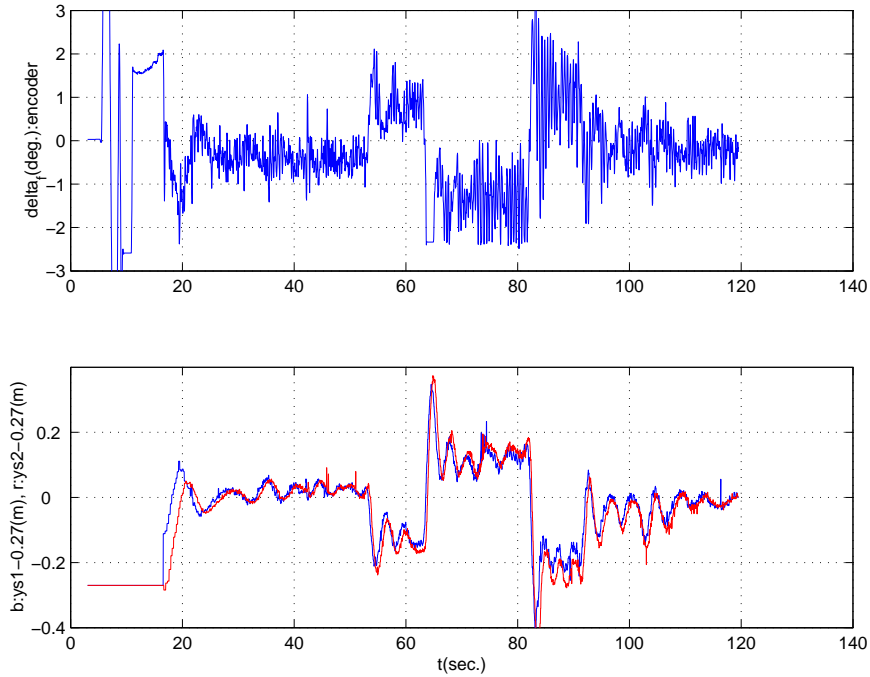Figure 28: Experimental results of Sliding Mode Controller–1

Figure 29: Experimental results of Sliding Mode Controller–2

manually give a large steering action guaranteeing the front steering wheel to pass through the "zero" position. The former is because, the current calibration algorithm implemented on our test vehicle is unreliable and often times it finds a wrong "zero" position. Whenever this happens, the steering command has to maintain a nonzero value at the straight road for the front steering wheel to point the actual "zero" position. This nonzero steering command is achieved by forcing the vehicle to have a constant lateral tracking error. Therefore, in the case that the calibration algorithm finds the correct "zero" position, the "ideal case", the actual tracking error should be the data shown by the plot (c)-s minus the steady state tracking error at the straight sections as shown in the lower plots of Figs. 25, 27 and 29. In the following, whenever we say a lateral tracking error, we refer to the "ideal" case. The upper plots of Figs. 25, 27 and 29 show the steering action of the steering column relative to the alleged "zero" position measured by the encoder.

The data for Figs. 24–27 are among the best experimental results of controllers A and B, respectively. For controler C, we could have done more experiments and

fine tuned the controller parameters if we have had more time on the day that we collected data for controllers A and B.

With controller A, the linear controller, the maximum velocity we could reach is about $50mph$, and the controller is very sensitive to the control parameters. Furthermore, the parameter range for which the controller can stabilize the vehicle lateral control system is very small. In other words, it can be said that controller A may not be able to stabilize the vehicle system when system parameters are changed. Therefore, controller A is not very robust.

However, with controller B, the linear controller with a feedforward compensation, the maximum velocity we could reach with a reasonable performance such as small oscillation is bout $55mph$, and the controller is not as sensitive as controller A to the controller parameters. Besides, controller B shows improved steady state tracking error ($16cm$) at the curved sections than controller A ($20cm$).

With controller C, the sliding mode controller, we could easily speed up $60mph$ without letting the vehicle go unstable or go out of the magnetometer measurement range. For the data shown in Fig. 29, the steady state lateral tracking error is about $12cm$, the best among the three controllers. The present experimental data of controller C show more oscillations than that of controllers A and B, but as we mentioned, there are possibility of tuning the control parameters for controller C such that it shows far better performance that of controller A and B.

5   Autonomous Following Control

5.1   Laser Scanning Radar Description and Geometry

Laser scanning radar, which is installed on the front of a following vehicle, emits infrared light that is reflected off patches on the rear of the preceding vehicle. These reflections give the distance and angle (r_i, α_i) to each reflective object on the preceding vehicle (distance and angle resolutions are 15 cm and 0.15^o, respectively). The effects

of false targets and reflective clutter are ignored, and the measurement is assumed to be reliable. Standard triangulation schemes allow the relative longitudinal and lateral distances and yaw angle of the preceding vehicle to be calculated as shown in Figure 30. Lines are drawn (L_l, L_r) from the reflective points on the preceding vehicle to the
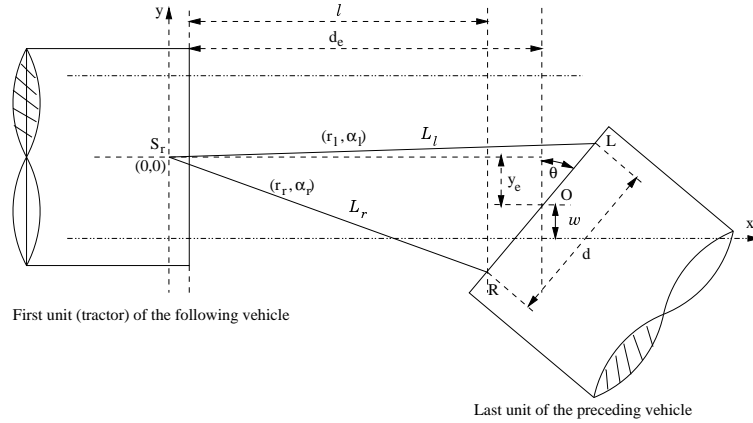

Figure 30: Laser scanning radar geometry

laser scanning radar unit. Using the equations of these lines in the coordinate frame, one can use geometric relations to obtain the relative displacements and yaw of the preceding trailer. The tracking algorithms presented depend on the relative lateral and longitudinal centerline positions (y_e and d_e) and the relative yaw (θ).

5.2 Linearized Vehicle Model for Autonomous Following

Dynamic modeling for a tractor-semi trailer vehicle can be found in [2] and [11]. The autonomous following vehicle dynamics are modeled in the unsprung mass reference frame with the origin at the tractor's center of gravity. Assuming negligible roll motion, small longitudinal acceleration, and small articulation angle between the tractor and semi-trailer, the linearized vehicle dynamic equations, similar to those

41

given by a bicycle model, can be written as

$$\frac{d}{dt}x = \begin{bmatrix} 0 & 0 & 0 & 1 & 0 \\ 0 & 0 & 0 & 0 & 1 \\ (-M^{-1}K) & (-M^{-1}D) \end{bmatrix} x + \begin{bmatrix} 0_{(2\times 1)} \\ (M^{-1}F) \end{bmatrix} \delta_{f1}$$
$$= Ax + B\delta_{f1} \tag{42}$$

where

$$x = \begin{bmatrix} x_1 & x_2 & x_3 & x_4 & x_5 \end{bmatrix}^T \tag{43}$$
$$= \begin{bmatrix} \epsilon_1 & \epsilon_{f1} & \dot{y}_{u1} & \dot{\epsilon}_1 & \dot{\epsilon}_{f1} \end{bmatrix}^T$$

The M,D,K, and F matrices are explained in Appendix C. ϵ_1 is the yaw angle of the tractor (subscript 1 represents the first vehicle) in the inertial reference frame, ϵ_{f1} is the articulation angle between the tractor and the trailer, and $\dot{y}_{u1}$ is the lateral velocity at the tractor CG. The front wheel steering angle is δ_{f1}. In addition to the plant dynamics, the system also contains steering actuator dynamics. The steering actuator, together with the steering inner loop controller, are modeled as a first order system that rolls off at a little less than 3 Hz. The dynamics of the steering actuator is represented by

$$SA(s) = \frac{18}{s + 18} \tag{44}$$

Estimated vehicle parameters used for the autonomous following analysis can be seen in Appendix B. The dynamic model given by [2] and [11] has been validated by experiments [16].

5.3   Modeling of Relative Lateral Displacement and Yaw

The behavior of the measured values given by the laser scanning radar system depends on the dynamics of the preceding and following vehicles. It is reasonable to assume that the vehicles will be traveling at the same longitudinal speed ($\dot{x}_u$), so the longitudinal distance between vehicles (d_e) will be assumed constant. The relative

42

lateral displacement (y_e) and yaw (θ), however, change as the two vehicles negotiate curves, and, thus, modeling these two parameters as functions of the vehicle states will be useful in developing a control model. Since the autonomous following controller will be implemented on the following vehicle, it is sensible to model the dynamics of y_e and θ with respect to the following vehicle dynamics and treat the motion of the preceding vehicle as a disturbance. Figure 31 shows the change in y_e and θ with respect to changes in the states of the following vehicle. The curvature of the pre-
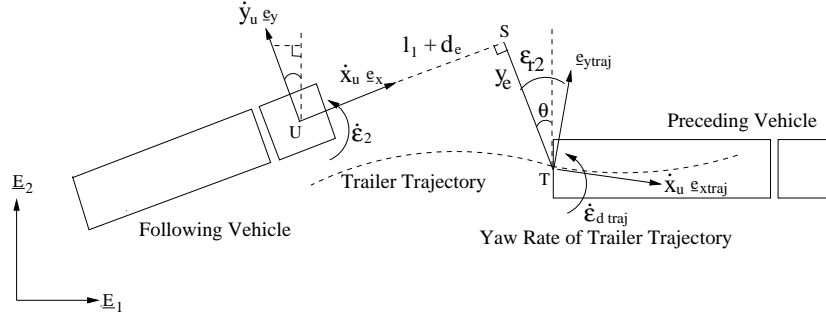

Figure 31: Dynamics of measured parameters, y_e and θ (l_1: distance between the following tractor's CG and the front bumper)

ceding trailer's trajectory can be described by a desired yaw rate, $\dot{\epsilon}_{d_{traj}}$, for a given longitudinal velocity of the heavy vehicles. This desired yaw rate and the yaw rate of the preceding trailer ($\dot{\epsilon}_1 + \dot{\epsilon}_{f1}$) are treated as disturbances to the laser scanning radar measurements.

$$\ddot{y}_e = \ddot{y}_u + (d_e + l_1)\ddot{\epsilon}_2 + \dot{x}_u \dot{\epsilon}_2 - \dot{x}_u \dot{\epsilon}_{d_{traj}} \tag{45}$$

$$\dot{\theta} = \dot{\epsilon}_2 - (\dot{\epsilon}_1 + \dot{\epsilon}_{f1}) := \dot{\epsilon}_2 + d_\theta(t) \tag{46}$$

Extending the state vector (43) with three new states (y_e, θ, and $\dot{y}_e$) and including the disturbance terms gives the following extended state space model.

$$x_{ext} = \begin{bmatrix} x & y_e & \theta & \dot{y}_e \end{bmatrix}^T \tag{47}$$

$$= \begin{bmatrix} \epsilon_1 & \epsilon_{f1} & \dot{y}_{u1} & \dot{\epsilon}_1 & \dot{\epsilon}_{f1} & y_e & \theta & \dot{y}_e \end{bmatrix}^T$$

$$d(t) = \begin{bmatrix} \dot{\epsilon}_{d_{traj}} & d_\theta(t) \end{bmatrix}^T \tag{48}$$

43

$$\dot{x}_{ext} = A_{ext}x_{ext} + B_{ext}\delta_{f2} + E_{ext}d(t) \tag{49}$$

5.4 Analysis of Relative Lateral Displacement and Yaw

The autonomous following controller will be implemented on the following vehicle using the laser scanning radar measurements. For this reason, a brief frequency domain analysis of the transfer functions $\frac{Y_e(s)}{\delta_{f2}(s)}$ and $\frac{\theta(s)}{\delta_{f2}(s)}$ is performed. Figures 32 and 33 show the Bode plots of the two transfer functions for varying velocity.
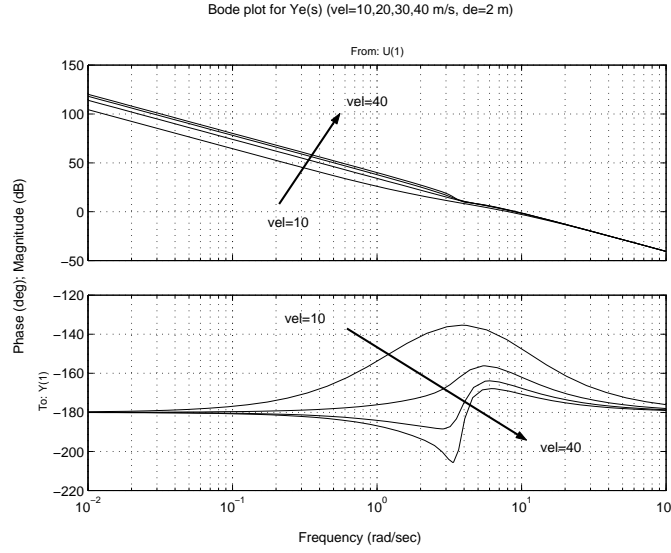

Figure 32: Bode plot of $\frac{Y_e(s)}{\delta_{f2}(s)}$ for varying longitudinal velocity $(\dot{x}_u)$ $(d_e = 2\ m)$

In the Bode plot of $\frac{Y_e(s)}{\delta_{f2}(s)}$, the low frequency gain increases with increased velocity, but the high frequency gain is unaffected by changing velocity. The phase angle does not reach (-180°) at low frequencies but exceeds (-180°) at frequencies lower than 5 rad/sec (0.8 Hz) for higher velocities. For $\dot{x}_u = 40\ m/s$ the phase lag peaks at 3.5 rad/sec (0.56 Hz). This behavior is similar to that of the virtual sensor defined at the look-ahead distance for magnetometer-based control [17]. For the Bode plot of $\frac{\theta(s)}{\delta_{f2}(s)}$, a peak in the magnitude appears at 3 rad/sec (0.48 Hz) as velocities exceed
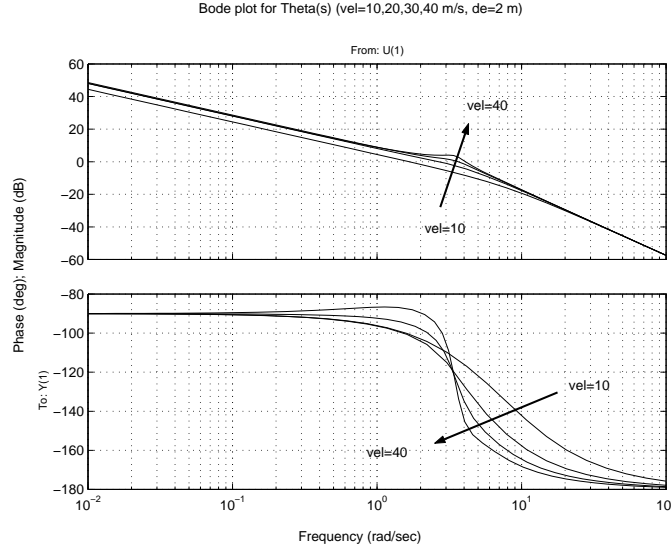
Figure 33: Bode plot of $\frac{\theta(s)}{\delta_{f2}(s)}$ for varying longitudinal velocity $(\dot{x}_u)$ $(d_e = 2\ m)$

$30\ m/s$. The phase plot exhibits lead as velocity increases for frequencies less than $3\ rad/sec$ (0.48 Hz), but the trend reverses at higher frequencies.

Figure 34 shows the Bode plot of $\frac{Y_e(s)}{\delta_{f2}(s)}$ for varying truck spacing. The gain of $\frac{Y_e(s)}{\delta_{f2}(s)}$ decreases with increasing frequency, and an increase in truck spacing causes a rise in the gain at frequencies above 1 rad/sec (0.16 Hz). The phase angle does not exceed (-180°) for all truck spacing distances, and larger truck spacing distances provide larger phase lead. As mentioned earlier, this behavior is similar to the phase advance given by the geometric look-ahead scheme used in magnetometer-based control [17]. $\frac{\theta(s)}{\delta_{f2}(s)}$ is not sensitive to changes in truck spacing, leaving its Bode plot unchanged by varying d_e.

5.5   Tracking Methods and Controller Designs

5.5.1   Minimizing Relative Lateral Distance

The first tracking method involves regulating the relative lateral distance (y_e) to zero, which is equivalent to linearly interpolating a trajectory between the following tractor and preceding trailer. The open loop Bode plot with and without the controller
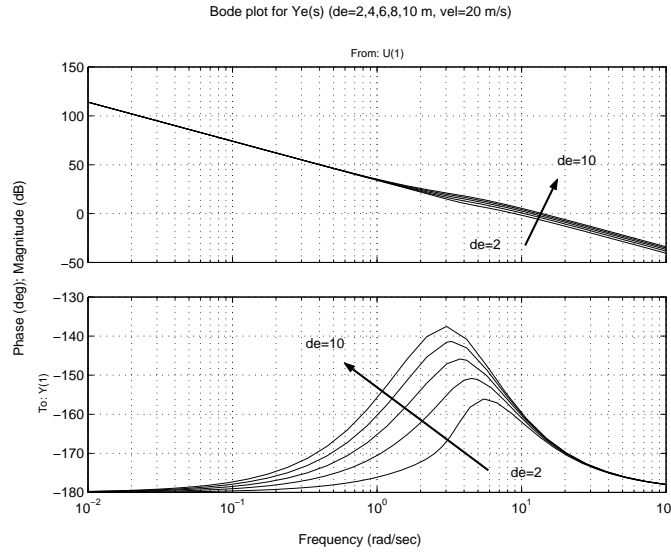
Figure 34: Bode plot of $\frac{Y_e(s)}{\delta_{f2}(s)}$ for varying truck spacing (d_e) $(\dot{x}_u = 20\ m/s)$

is shown in Figure 35. The controller gives the open loop a phase margin of 32° and moves the gain crossover frequency to 6.35 rad/sec (1 Hz). It is designed so that motion above the 1-2 Hz range is minimized, because this can cause passenger discomfort.

5.5.2 Minimizing Projected Lateral Error using Yaw Rate Control

A second tracking method involves using a contour of constant curvature to interpolate a trajectory between the following tractor and preceding trailer. If the tractor is traveling with constant yaw rate and longitudinal velocity, the trajectory of the CG is approximately a circular path. This fact is used to interpolate a constant curvature reference between the following tractor and preceding trailer. The projected lateral displacement of the following tractor's CG at the end of this curve is defined as y_p. Regulating y_p using the measurement, y_e, at the distance $(d_e + l_1)$ from the following tractor's CG defines a desired yaw rate to follow the interpolated curve [14]. The geometry of the projected lateral displacement is shown in Figure 36, and the
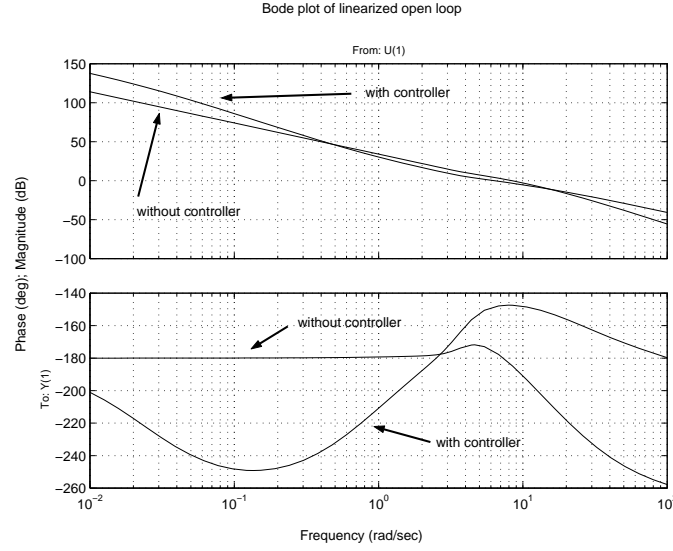
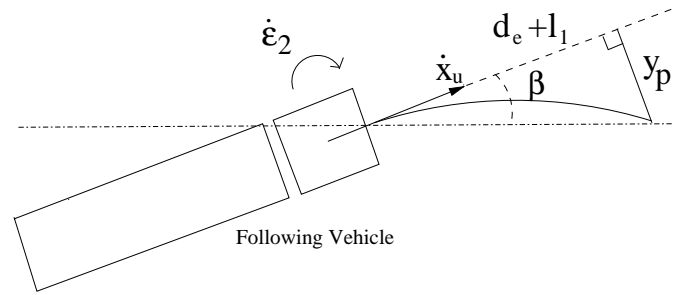Figure 35: Open loop Bode plot for linear interpolation ($\dot{x}_u = 20 \ m/s, d_e = 2 \ m$)

Figure 36: Projected lateral displacement geometry

parameters are described below.

$$\beta = \frac{\dot{\epsilon}_2 t_p}{2} \tag{50}$$

where t_p is the time to travel through the distance $(d_e + l_1)$.

$$t_p \approx \frac{d_e + l_1}{\dot{x}_u} \tag{51}$$

The projected lateral displacement of the vehicle at $(d_e + l_1)$ is

$$y_p = -(d_e + l_1)tan(\beta) \tag{52}$$

The variable y_p is defined to be positive and $\dot{\epsilon}_2$ is negative for the situation shown in Figure 36. For this reason, a negative sign appears in Equation (52). Setting

47

$y_p - y_e = 0$ gives the following expression for the desired yaw rate of the following vehicle that results in the desired projected lateral displacement.

$$\dot{\epsilon}_{2_{desired}} = -\frac{2\dot{x}_u}{d_e + l_1} tan^{-1}\left(\frac{y_e}{d_e + l_1}\right) \tag{53}$$

The (tan^{-1}) function can be linearized, because $y_e << (d_e + l_1)$ during autonomous following control. Figure 37 shows the open loop Bode plot from steering input to yaw rate error $(\dot{\epsilon}_2 - \dot{\epsilon}_{2_{desired}})$ for projected lateral error minimization with and without the controller $(d_e = 2\ m, \dot{x}_u = 20\ m/s)$. Including the controller in the open loop gives a
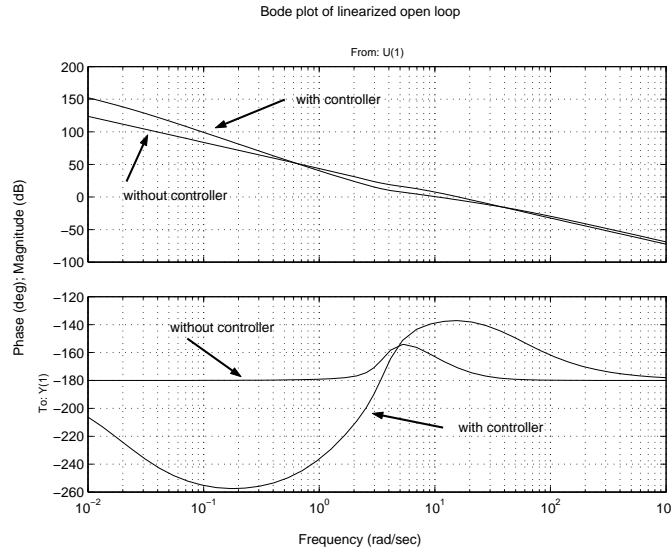

Figure 37: Open loop Bode plot for constant curvature interpolation $(\dot{x}_u = 20\ m/s, d_e = 2\ m)$

phase margin of 41° and moves the gain crossover frequency to $10.6\ rad/sec$ $(1.68\ Hz)$.

5.5.3 Preceding Tractor Location using Relative Yaw

One obvious problem is that the visual sensing system can only give information about the rear of the preceding trailer, which may not follow the path of the preceding tractor's CG (trailer offtracking). With knowledge of the trailer length (l_3), the relative yaw (θ) can be used to obtain the relative lateral and longitudinal distances to the 5th wheel (hitch) of the preceding tractor (see Figure 38). As stated earlier,
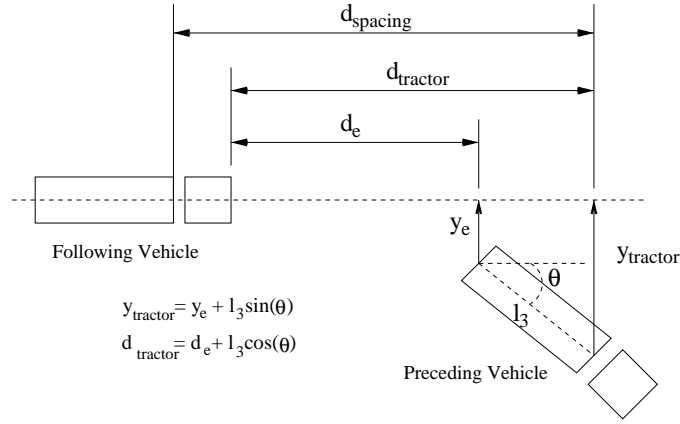
Figure 38: Using relative yaw to find the relative lateral and longitudinal distances to the preceding tractor

one problem with this method is that during highway operation, the relative yaw can be quite small, making measurement resolution a problem. For this reason, it may be difficult to implement a controller based on the projected tractor position, but simulations of this type of control can show a best possible case for tracking within the platoon. Since constant curvature interpolation is more robust to the additional spacing introduced when tracking the previous vehicle's 5th wheel, compared to linear interpolation, it will be the reference generation method used for this case. The projected displacement of the 5th wheel, y_{d1}, is found to be

$$y_{d1} = -d_{spacing} tan\left(\frac{\dot{\epsilon}_2 t_p}{2}\right) + d_1 sin(\dot{\epsilon}_2 t_p) \tag{54}$$

where $d_{spacing}$ is the distance between the 5th wheels of the preceding and following vehicles, and d_1 is the distance between the tractor's CG and its 5th wheel. The second term on the right side of Equation (54) is the difference between y_p of the tractor's CG and the projected lateral displacement of its 5th wheel after the truck has rotated along the curve. As in projected lateral error control, setting $y_{d1} - y_{tractor} = 0$ gives an expression for the desired yaw rate of the following vehicle (small angle assumptions allow for the linearization of the trigonometric functions). The controller design and resulting open loop dynamics are similar to those developed for projected lateral error control.
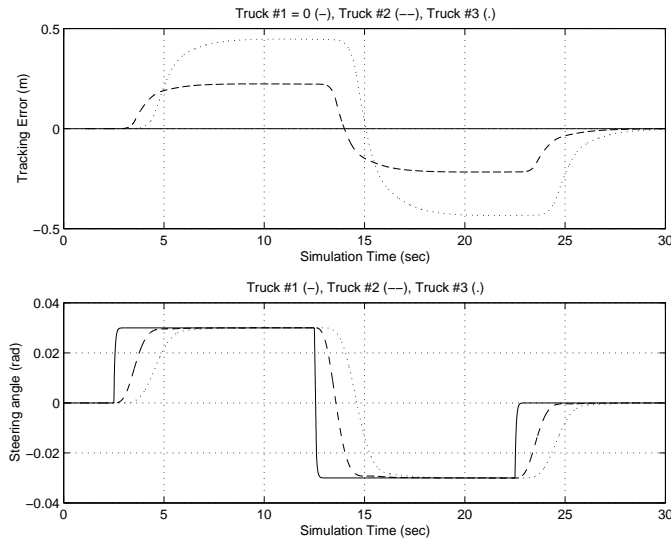
49

Figure 39: Steering responses and tracking errors of the tractor CG's for a three vehicle platoon simulation using relative lateral distance minimization, $d_e = 10\ m$ ($\dot{x}_u = 20\ m/s$)

5.6 Simulations and Results

Simulations are performed with three heavy vehicles in a 2-D plane with the first vehicle starting at the origin of the plane and each successive vehicle following d_e meters behind the preceding trailer at the same longitudinal velocity ($\dot{x}_u = 20\ m/s$). The visual sensor parameters are calculated using the absolute position of the preceding trailer and following truck in the 2-D space. The initial steering angle input to the front wheels of the leading vehicle is zero, followed by a 1.7^o input after $t = 2.5\ sec$, and switched to -1.7^o at $t = 12.5\ sec$. The input is again set to zero at $t = 22.5\ sec$.

5.6.1 Minimizing Relative Lateral Distance

The tracking error is defined as the position of each following tractor's CG along the perpendicular to the trajectory of the first tractor's CG in the 2-D plane. For small truck spacing distances, such as $d_e = 2\ m$, the tracking error is quite small, but it becomes large for larger truck spacing distances (see Figure 39). The large steady state tracking error exists, because the trucks tend to "cut" the corners of the
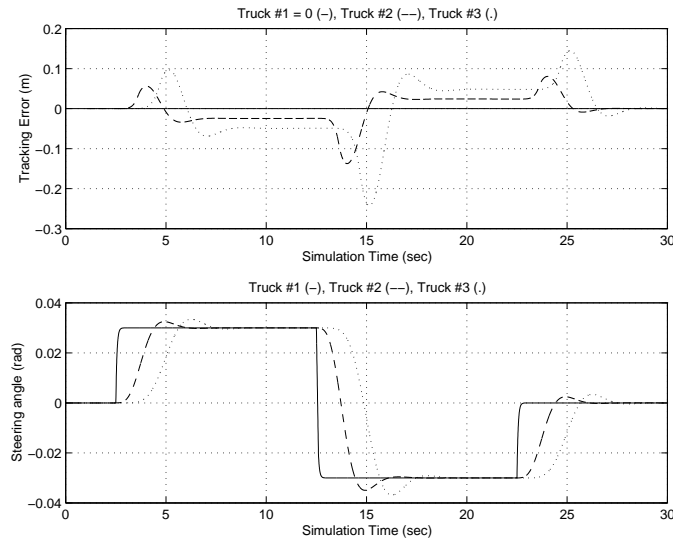
Figure 40: Steering responses and tracking errors of the tractor CG's for a three vehicle platoon simulation using projected lateral error minimization, $d_e = 10\ m$ $(\dot{x}_u = 20\ m/s)$

preceding trailer's trajectory when the truck spacing is increased to 10 m while using the linear interpolation method.

5.6.2   Minimizing Projected Lateral Error using Yaw Rate Control

Figure 40 shows the tracking errors and steering responses of the two following vehicles for $d_e = 10\ m$ using projected lateral error minimization, where the tracking error is as stated above. The error is quite small for $d_e = 2\ m$, and the steady state error remains small when the truck spacing is increased to 10 m. As one would expect, this method is more robust to changes in truck spacing than the linear interpolation method. Since the vehicle has some side slip and the preceding trailer does not necessarily follow the same path as the preceding tractor's CG (trailer offtracking), some steady state error is to be expected.

5.6.3 Preceding Tractor Location using Relative Yaw

Figure 41 shows the tracking errors and steering angles for the two following vehicles using the projected position of the preceding tractor's 5th wheel as the reference. It is important to note that the interpolation is performed over a distance of $d_{spacing} \approx$ 13.5/m ($d_e = 2\ m$) for this simulation. The tracking is quite good (steady state error ≤ 3 cm for the third platoon vehicle) using this method, but these results are based on the assumption that the relative yaw measurement is clean and that model uncertainty is at a minimum. Although this method may not be implementable due to poor resolution of the relative yaw measurement, the simulation shows the importance of eliminating the trailer offtracking behavior from the generation of the reference trajectory.
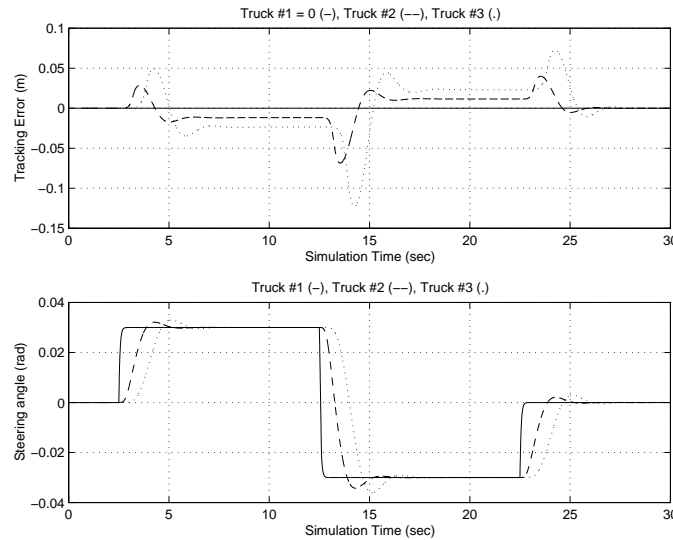

Figure 41: Steering responses and tracking errors of the tractor CG's for a three vehicle platoon simulation using relative yaw to find the position of the preceding tractor, $d_{spacing} \approx 13.5/m$ ($\dot{x}_u = 20\ m/s$)

5.7 Trajectory Storage

Storing the trajectory of the preceding vehicle eliminates the controller dependence on truck spacing distance [15]. The relative position of the preceding vehicle is given in the unsprung mass reference frame by (d_e, y_e). These positions can be discretely stored and rotated and translated as the following vehicle travels [13]. The relative position of the stored point in the unsprung mass reference frame can then be used by the controller when it is near the point to be controlled on the following vehicle. For example, a point on the trajectory can be stored until the "x" value of the point becomes zero in the unsprung mass reference frame. This means that the point is even with the CG of the following vehicle, and the "y" value of the point can be used as the tracking error (input to the controller). The trajectory storage device can be represented by a discrete time system that rotates and translates each point $(k-1)$ based on the motion of the following vehicle and stores this value as the new point (k). Equation 55 shows the calculation of each point using the previous point $(k-1)$, longitudinal velocity $(\dot{x}_u)$, lateral velocity $(\dot{y}_u)$, and yaw rate $(\dot{\epsilon}_1)$ of the following vehicle, and the sample time (Δt).

$$
\begin{aligned}
x(k) &= (-\dot{\epsilon}_1 y(k-1) - \dot{x}_u)\Delta t + x(k-1) \\
y(k) &= (\dot{\epsilon}_1 x(k-1) + \dot{y}_u)\Delta t + y(k-1)
\end{aligned}
\tag{55}
$$

If the lateral velocity cannot be estimated, $\dot{y}_u$ is assumed to be zero. The trajectory storage device allows for the development of new tracking strategies.

5.8 Trailer Position Control

With the stored trajectory of the preceding trailer now available in the unsprung mass reference frame, it is sensible to control the following trailer position to follow this trajectory. While the propagation of tracking errors throughout a platoon of vehicles can be reduced using this method, the ability to control trailer acceleration is limited.

The development of a control model for trailer trajectory tracking requires the definition of a reference frame that moves along the desired trajectory at the same longitudinal velocity as the trailer, i.e. the trajectory reference frame ($\underline{e}_{x_{traj}}$, $\underline{e}_{y_{traj}}$). A trailer reference frame will be defined at the rear of the trailer ($\underline{e}_{x_t}$, $\underline{e}_{y_t}$), and the relative yaw of the trailer reference frame to the trajectory reference frame will be defined as ϵ_{rt}. The position of the trailer in the trajectory reference frame, defined as y_t, represents the error quantity that the controller must regulate. Figure 42 shows the geometry for the trailer trajectory tracking control model. The relative yaw rate
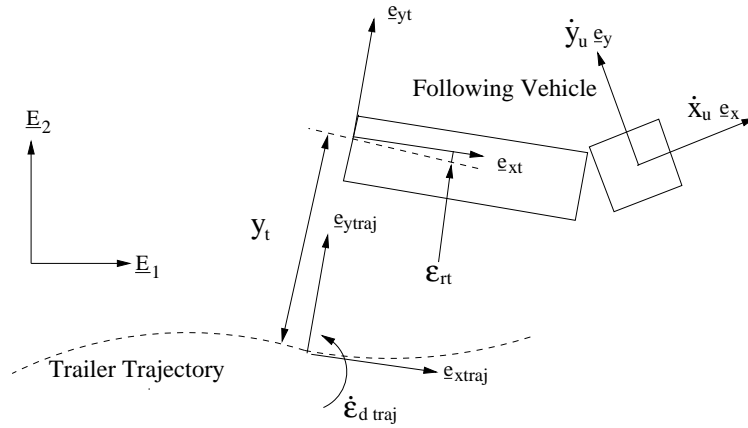

Figure 42: Trailer trajectory tracking geometry

of the following trailer to the desired trajectory is

$$\dot{\epsilon}_{rt} = \dot{\epsilon}_2 + \dot{\epsilon}_{f2} - \dot{\epsilon}_{d_{traj}} \tag{56}$$

where $\dot{\epsilon}_{d_{traj}}$ is the desired yaw rate of the trajectory, similar to that defined in Equation 45. An expression for trailer velocity in the $\underline{e}_{y_{traj}}$ direction ($\dot{y}_t$) can be derived in terms of the relative trailer yaw to the trajectory and the vehicle states defined in Section 5.2. Assuming small articulation angle and longitudinal acceleration, the expression for trailer lateral velocity in the trajectory reference frame is

$$\dot{y}_t = \dot{y}_u + \dot{x}_u \epsilon_{rt} - \dot{x}_u \epsilon_{f2} - (d_1 + l_3)\dot{\epsilon}_{rt} + d_1 \dot{\epsilon}_{f2} - (d_1 + l_3)\dot{\epsilon}_{d_{traj}} \tag{57}$$

Extending the vehicle state space model with the equations for $\dot{\epsilon}_{rt}$ and $\ddot{y}_t$ gives a linear model for the dynamics in the trajectory reference frame.

Figure 43 shows the Bode plot of the transfer function from steering input to trailer lateral position in the trajectory reference frame. As frequency increases, the phase lag increases significantly, making the system very difficult to control with higher bandwidth controllers. Lower bandwidth controllers have large tracking errors due to the slow response of the controller to changes in the reference trajectory. The undamped zero pair evident from the notch also presents a problem, because it appears in a critical frequency region.
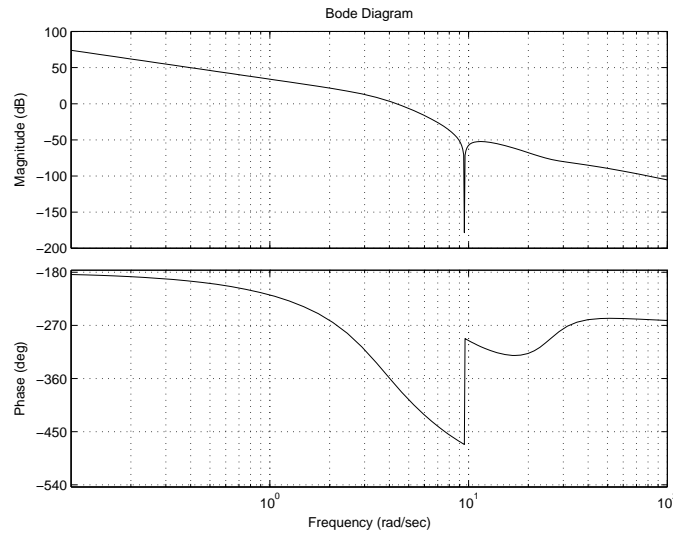

Figure 43: Bode plot of transfer function from steering input to trailer lateral position in the trajectory reference frame (linearized expression) ($\dot{x}_u = 20 \ m/s$)

Further insight into the dynamic behavior of the trailer can be gained by redefining the error using the previously defined y_e where $d_e = -d_1 - l_3 - l_1$ from the laser scanner location at the front of the tractor. This is equivalent to fictitiously placing the preceding trailer to be tracked next to the following trailer, eliminating the time lag created by the trajectory storage device. The equation for tracking error then becomes

$$y_{error} = y_e - l_3 sin(\epsilon_{f2}) \tag{58}$$

The Bode plot from steering input to this newly defined error is identical to that shown in Figure 43. The existence of the notch can be understood by looking at

55

the Bode plots of the transfer functions from steering input to y_e and to $-l_3\epsilon_{f2}$ as shown in Figure 44. The magnitudes of the two transfer functions are the same
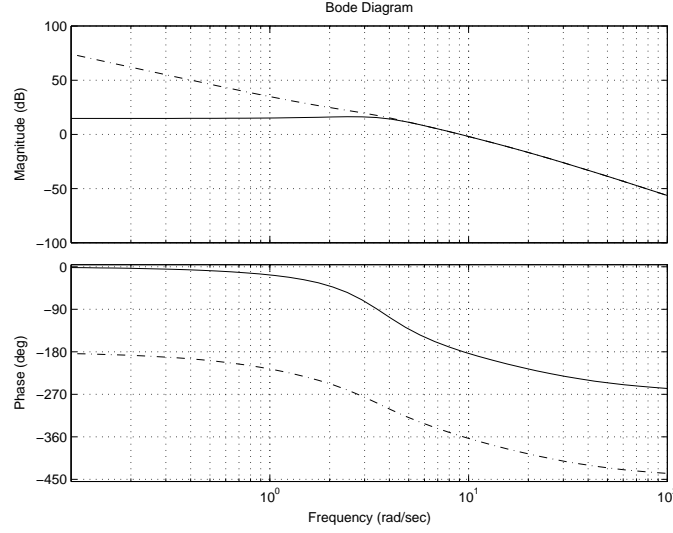

Figure 44: Bode plot of transfer function from steering input to y_e (dashed line) and $-l_3\epsilon_{f2}$ (solid line) ($\dot{x}_u = 20 \ m/s$)

at frequencies above 5 rad/sec, and the frequency where the phase angles differ by exactly 180° determines the location of the notch. One way to overcome the significant phase lag and the notch introduced by the trailer dynamics is to add a look-ahead distance similar to that done in magnetometer-based control (d_{st}), thus, d_e and y_{error} are redefined as

$$d_e = -d_1 - l_3 - l_1 + d_{st} \tag{59}$$

$$y_{error} = y_e + (-l_3 + d_{st})sin(\epsilon_{f2}) \tag{60}$$

Further research into the trailer behavior and controller design is required before conclusions can be drawn.

6 Conclusions

The improvement of yaw stability of the trailer by using the proposed steering and differential braking controller has been shown. The controller is robust to parameter

uncertainties including vehicle longitudinal speed, road adhesion coefficient, and cargo loads in the trailer. The measurements required for the synthesis of control inputs are available from the existing sensors on the experimental truck. This feature provides an easy implementation of the proposed controller.

The experimental results show that, the addition of the feedforward compensator to the linear feedback control system lifts the performance upper limit of the linear feedback control system and improves the system performance without adding too much complexity in the implementation and tuning of the control parameters. On the other hand, while the sliding mode controller seemingly lifts the upper limit of the linear feedback control system with feedforward compensation, the implementation induces other issues such as careful system identification and observer design, and the tuning of the control parameters is not a trivial task. It is concluded that a feedforward compensation in addition to a robust linear feedback controller is a midpoint between nonlinear controllers and linear robust controllers in terms of the ease of implementation and the improved control system performance.

For autonomous following lateral control, expressions were obtained for the useful measured variables of the laser scanning radar unit (y_e and θ) by treating the motion of the preceding vehicle as a disturbance. A frequency domain analysis was performed on these two variables. Two of the presented tracking methods used linear and constant curvature interpolations, respectively, to define the desired trajectory for the following tractor's CG. A third method used constant curvature interpolation to track the preceding tractor's 5th wheel with the same point on the following vehicle. The constant curvature interpolation method makes the steady state tracking error robust to changing vehicle spacing (compared to linear interpolation), and the tracking error can be significantly reduced when the offtracking behavior of the trailer is eliminated from the generation of the reference trajectory. The trajectory of the preceding trailer can also be discretely stored and used as a tracking reference for the following trailer. The notch behavior and significant phase lag of the trailer dynamics pose an

interesting problem for linear controller design, requiring more study.

Acknowledgement

References

[1] J.-Y. Wang and M. Tomizuka, "Analysis and Controller Design Based on Linear Model for Heavy-Duty Vehicles", *International Mechanical Engineering Congress & Exposition, ASME Symposium on Transportation Systems, Anaheim, CA*, pp. 729-735, 1998

[2] C. Chen and M. Tomizuka, "Dynamic Modeling of Articulated Vehicles for Automated Highway Systems", *Proc. of American Control Conference, Seattle, WA*, pp. 653-657, 1995.

[3] J.-Y. Wang and M. Tomizuka, "Robust H_∞ Lateral Control for Heavy-Duty Vehicles in Automated Highway System", *Proc. of American Control Conference, San Diego, CA*, pp. 3671-3675, 1999.

[4] P. Hingwe, M. Tai, J.-Y. Wang and M. Tomizuka, "Lateral Control of Tractor-Semitrailer Combination for Automated Highway Systems–An Experimental Study", *International Mechanical Engineering Congress & Exposition, ASME Symposium on Transportation Systems*, 1999.

[5] S. Patwardhan, H.-S. Tan, and J. Guldner, "A general Framework for Automatic Steering Control: System Analysis", *Proc. of American Control Conference*, Albuquerque, New Mexico, pp.1598-1602, 1997.

[6] S. Mammar, "Robust Reduced Order Two-Degree-of-Freedom Tractor-Semitrailer Lateral Control", *Proc. of American Control Conference, San Diego, CA*, pp. 3158-3162, 1999.

[7] P. Kapasouris, "Gain-Scheduled Multivariable Control for the GE-21 Turbofan Engine Using the LQG and LQG/LTR Methodology", Master's thesis, Massachusetts Institute of Technology, 1984.

[8] J.A. Sefton and K. Glover, "Pole/Zero Cancellations in the General H_∞ Problem with Reference to a Two Block Design", *System and Control Letters*, 14: pp295-306, 1990.

[9] R.A. Hyde, "H_∞ Aerospace Control Design–A VSTOL Flight Application", Springer 1995.

[10] D.J. Stilwell and W.J. Rugh, "Interpolation of Observer State Feedback Controllers for Gain-Scheduling", *Proc. of American Control Conference, Philadelphia, PN*, pp. 1215-1219, 1998.

[11] C. Chen, "Backstepping Design of Nonlinear Control Systems and Its Application to Vehicle Lateral Control in Automated Highway Systems", Ph.D. dissertation, UC Berkeley.

[12] X. Claeys, C. Canudas de Wit, and H. Béchart, "Lateral Control of Heavy-Duty Vehicles in a Convoy", 2000.

[13] R. Frezza and G. Picci, "On line path following by recursive spline updating", *Proceedings of the 34th Conference on Decision & Control, New Orleans, LA*, pp. 4047-4052, 1995.

[14] T. Fujioka and M. Omae, "Vehicle Following Control in Lateral Direction for Platooning", *Vehcile System Dynamics Supplement 28*, pp. 422-437, 1998.

[15] S. Gehrig and F. Stein, "A Trajectory-Based Approach for the Lateral Control of Car Following Systems", *Proceedings of the Intelligent Vehicles Symposium '98*, pp. 3596-3601, 1998.

[16] P. Hingwe, J.-Y. Wang, M. Tai, and M. Tomizuka, "Lateral Control of Heavy Duty Vehicles for Automated Highway System: Experimental Study on a Tractor Semi-trailer", California PATH Working Paper, UCB-ITS-PWP-2000-1, 2000.

[17] J.-Y. Wang and M. Tomizuka, "Dynamics Analysis and Robust Steering Controller Design for Automated Lane Guidance of Heavy-Duty Vehicles", *Asian Journal of Control*, Vol. 2, No. 3, pp. 140-154, September 2000.

[18] M. Tomizuka, M. Tai, J-Y. Wang and P. Hingwe, (1999). "Automated Lane Guidance of Commercial Vehicles," Proceedings of the 1999 IEEE International Conference of Control Applications, pp. 1359-1364, Hawaii, August 1999.

[19] C. Chen and M. Tomizuka, (1995). Steering and Independent Braking Control of Tractor-semitrailer Vehicle in Automated Highway Systems. Proc. of IEEE Conference on Decision and Control, New Orleans, 1561-1566.

[20] M. Tai and M. Tomizuka, (1999). "Robust Lateral Control of Heavy Duty Vehicles for Automated Highway Systems," Proceedings of the 14th IFAC World Congress, Vol. Q, pp. 37-42, Beijing, China, July 1999.

[21] J. Ackermann, J. Guldner, W. Sienel, R. Steinhauser, (1995). "Linear and Nonlinear Controller Design for Robust Automatic Steering," *IEEE Trans. on Control Systems Technology,*, Vol 3, pp. 132-143.

[22] P. Hingwe and M. Tomizuka, (1995). "Two Alternative Approaches to the Design of Lateral Controllers for Commuter Buses based on Sliding Mode Control,"

ASME International Mechanical Engineering Congress and Exposition, DSC-vol.56/DE-vol.86, pp.99-104.

[23] M. Krstic, I. Kanellakopoulos and P. V. Kokotovic, (1995). " Nonlinear and Adaptive Control Design," New York: Wiley.

[24] M. Tai and M. Tomizuka, (1998). "Dynamic Modeling of Multi-Unit Heavy Vehicles," Proceeding of the 1998 International Mechanical Engineering Congress and Exposition, DSC-Vol. 64, pp. 673-680, Anaheim, November 1998.

[25] P. Hingwe, M. Tai and M. Tomizuka, (1999). "Modeling and Robust Control of Power Steering System of Heavy Vehicles for AHS," Proceedings of the 1999 IEEE International Conference of Control Applications, pp. 1365-1370, Hawaii, August 1999.

[26] J.-Y. Wang and M. Tomizuka, (2000). "Coordinated Steering and Differential Braking Control for Tractor-Semitrailer Combination Vehicles," Proceeding of the 2000 International Mechanical Engineering Congress & Exposition, Orlando, FL, December 2000.

[27] S. Skogestad and I. Postlethwaite, (1996). "Multivariable Feedback Control - Analysis and Design," John Wiley & Sons, 1996.

[28] M. Flick, (1990). "Stopping Distance of 1988 Heavy Vehicles," NHTSA's Heavy-Duty Vehicle Brake Research Program, no. 9, 1990.

[29] R. Limpert, (1992). "Brake Design and Safety," Society of Automotive Engineers, Inc., 1992.

Appendix

A The Linearized Model in the Road Reference Frame

1. The inertia matrix M is

$$
M = \begin{bmatrix} m_1 + m_2 & -m_2(d_1 + d_3) & -m_2 d_3 \\ -m_2(d_1 + d_3) & I_{z1} + I_{z2} + m_2(d_1^2 + d_3^2) + 2m_2 d_1 d_3 & I_{z2} + m_2 d_3^2 + m_2 d_1 d_3 \\ -m_2 d_3 & I_{z2} + m_2 d_3^2 + m_2 d_1 d_3 & I_{z2} + m_2 d_3^2 \end{bmatrix}
$$

2. The damping matrix D is

$$
D = \frac{2}{V_x} \begin{bmatrix} C_{\alpha f} + C_{\alpha r} + C_{\alpha t} & l_1 C_{\alpha f} - l_2 C_{\alpha r} - (l_3 + d_1)C_{\alpha t} & -l_3 C_{\alpha t} \\ l_1 C_{\alpha f} - l_2 C_{\alpha r} - (l_3 + d_1)C_{\alpha t} & l_1^2 C_{\alpha f} + l_2^2 C_{\alpha r} + (l_3 + d_1)^2 C_{\alpha t} & l_3(l_3 + d_1)C_{\alpha t} \\ -l_3 C_{\alpha t} & l_3(l_3 + d_1)C_{\alpha t} & l_3^2 C_{\alpha t} \end{bmatrix}
$$

3. The stiffness matrix K is

$$
K = 2 \begin{bmatrix} 0 & -(C_{\alpha_f} + C_{\alpha_r} + C_{\alpha_t}) & -C_{\alpha_f} \\ 0 & -(l_1 C_{\alpha_f} - l_2 C_{\alpha_r} - (l_3 + d_1)C_{\alpha_t}) & (l_3 + d_1)C_{\alpha_t} \\ 0 & l_3 C_{\alpha_t} & l_3 C_{\alpha_t} \end{bmatrix} .
$$

4. The vector F is

$$
F = \begin{bmatrix} 2C_{\alpha f} \\ 2C_{\alpha f} l_{f1} \\ 0 \end{bmatrix} . \tag{61}
$$

5. The vectors E_1 and E_2 are

$$E_1 = \begin{bmatrix} -\frac{2}{V_x}(l_1 C_{\alpha f} - l_2 C_{\alpha r} - (l_3 + d_1)C_{\alpha t}) - (m_1 + m_2)V_x \\ -\frac{2}{V_x}(l_1^2 C_{\alpha f} + l_2^2 C_{\alpha r} + (l_3 + d_1)^2 C_{\alpha t}) + m_2(d_1 + d_3)V_x \\ -\frac{2}{V_x}(l_3(l_3 + d_1)C_{\alpha t}) + m_2 d_3 v \end{bmatrix}$$

$$E_2 = \begin{bmatrix} m_2(d_1 + d_3) \\ -(I_{z1} + I_{z2} + m_2(d_1 + d_2)^2) \\ -(I_{z2} + m_2 d_3^2 + m_2 d_1 d_3) \end{bmatrix}.$$

B Nominal Parameters

Symbols	Definitions (Nominal Value)
m_1	tractor mass (7727 kg)
m_2^*	semitrailer mass (10455 kg)
d_1, d_2	relative position (x,y) between tractor's C.G. to fifth wheel (3.26 m, 0.60 m)
d_3, d_4	relative position (x,y) between semitrailer's C.G. to fifth wheel (3.81 m, 1.20 m)
I_{z1}	tractor yaw moment of inertia (45926 kgm^2)
I_{z2}^*	semitrailer yaw moment of inertia (161780 kgm^2)
l_1	distance between tractor C.G. and front wheel axle (1.61 m)
l_2	distance between tractor C.G. and rear wheel axle (3.75 m)
l_3	distance between joint (fifth wheel) and semitrailer wheel axle (6.50 m)
μ^*	road adhesion coefficient (1.0)
	(0.5 for wet road; 1.0 for dry road)
$C_{\alpha f}^*$	cornering stiffness of tractor front wheel (180430.0 $\times \mu$ N/rad)
$C_{\alpha r}^*$	cornering stiffness of tractor rear wheel (324774.0 $\times \mu$ N/rad)
$C_{\alpha t}^*$	cornering stiffness of semitrailer rear wheel (324774.0 $\times \mu$ N/rad)

C The Linearized Model in the Unsprung Mass Reference Frame

1. The inertia matrix M is

$$
M = \begin{bmatrix}
m_1 + m_2 & -m_2(d_1 + d_3) & -m_2 d_3 \\
-m_2(d_1 + d_3) & I_{z1} + I_{z2} + m_2(d_1^2 + d_3^2) + 2m_2 d_1 d_3 & I_{z2} + m_2 d_3^2 + m_2 d_1 d_3 \\
-m_2 d_3 & I_{z2} + m_2 d_3^2 + m_2 d_1 d_3 & I_{z2} + m_2 d_3^2
\end{bmatrix}
$$

2. The damping matrix D is

$$
D = \frac{2}{V_x} \begin{bmatrix}
C_{\alpha f} + C_{\alpha r} + C_{\alpha t} & l_1 C_{\alpha f} - l_2 C_{\alpha r} - (l_3 + d_1)C_{\alpha t} + (m_1 + m_2)\dot{x}_u & -l_3 C_{\alpha t} \\
l_1 C_{\alpha f} - l_2 C_{\alpha r} - (l_3 + d_1)C_{\alpha t} & l_1^2 C_{\alpha f} + l_2^2 C_{\alpha r} + (l_3 + d_1)^2 C_{\alpha t} - m_2(d_1 + d_3)\dot{x}_u & l_3(l_3 + d_1)C_{\alpha t} \\
-l_3 C_{\alpha t} & l_3(l_3 + d_1)C_{\alpha t} - m_2 d_3 \dot{x}_u & l_3^2 C_{\alpha t}
\end{bmatrix}
$$

3. The stiffness matrix K is

$$
K = 2 \begin{bmatrix}
0 & -C_{\alpha t} \\
0 & (l_3 + d_1)C_{\alpha t} \\
0 & l_3 C_{\alpha t}
\end{bmatrix}
$$

4. The vector F is

$$
F = 2C_{\alpha f} \begin{bmatrix}
1 \\
l_1 \\
0
\end{bmatrix}
$$